energies

MDPI

Article

Energy, Exergy, and Exergoeconomic Assessment of a Combined-Cycle Power Plant

Gustavo Basílio Lima, Júlia Alves Santos, Lucas Haas, Jocélio Jairo Vieira Filho, José Vinícius Santos de Araújo, João Alves de Lima, Gilberto Augusto Amado Moreira, Ademar Virgolino da Silva Netto, Sidneia Lira Cavalcante, Juan Moises Mauricio Villanueva, Euler Cássio Tavares de Macedo and Taynara Geysa Silva do Lago *

Renewable and Alternative Energy Center (CEAR), Federal University of Paraiba (UFPB), Cidade Universitária, João Pessoa 58051-970, Paraíba, Brazil; jalima@cear.ufpb.br (J.A.d.L.); gilberto@cear.ufpb.br (G.A.A.M.); ademar@cear.ufpb.br (A.V.d.S.N.); jmauricio@cear.ufpb.br (J.M.M.V.); euler@cear.ufpb.br (E.C.T.d.M.)
* Correspondence: taynara@cear.ufpb.br

Abstract

Combined-cycle gas turbine (CCGT) power plants play an important role in reducing greenhouse gas emissions while maintaining high thermal efficiency. Accurate thermodynamic models are essential for evaluating plant performance under different operating conditions and supporting improvements in energy resource management. This study presents a Python-based thermodynamic model of an isolated natural gas-fired CCGT power plant, applied to 1027 steady-state operating points recorded over one month of operation. The model integrates energy, exergy, and exergoeconomic analyses based on the Specific Exergy Costing (SPECO) methodology to assess plant operation with and without supplementary firing. The model was validated against the measured steam production, with a mean absolute percentage error of 2.8%. The proposed methodology enables the evaluation of component efficiencies, exergy destruction, cost formation, and the influence of different operating modes on electricity production. The plant achieved median gross first- and second-law efficiencies of 46.6% and 44.6%, respectively (45.1% and 43.2% on a net basis). The combustion chamber exhibited the highest exergy destruction in both operating modes, while the supplementary burner became one of the major sources of irreversibility when supplementary firing was activated. The specific exergy cost of electricity decreased from about 21.0 to 14.2 $/GJ as the electrical output increased from 11.3 to 20.9 MW, with a median of 16.47 $/GJ in the period. The supplementary burner presented the highest relative cost difference (median of 1.06), whereas the combustion chamber had the highest exergy destruction rate and cost rate of exergy destruction. The proposed model provides a flexible and reproducible framework for evaluating CCGT power plants and can support operational assessment and decision-making aimed at improving thermodynamic and economic performance.

Keywords: combined cycle; energy; exergy; thermodynamic model; python

Check for updates

Academic Editor: Jan Taler

Received: 17 September 2026
Revised: 19 October 2026
Accepted: 21 October 2026
Published: 3 November 2026

Copyright: © 2026 by the authors. Licensee MDPI, Basel, Switzerland. This article is an open access article distributed under the terms and conditions of the Creative Commons Attribution (CC BY) license.

1. Introduction

The assessment report published in 2022 by the IPCC indicates that a global temperature increase of 1.5 °C will be reached before 2040 if greenhouse gas emissions continue to rise uncontrollably [1]. In this scenario, strategies for safe and sustainable electrification

and for a more rational and efficient use of the available energy resources are highly relevant. Sustainable development therefore requires not only the reduction of greenhouse gas emissions but also solutions that improve the performance of power generation.

In the context of thermal power generation, natural gas is an attractive fuel option due to its lower CO_2 emissions compared with other fossil fuels, particularly coal and oil. Its use is especially advantageous in combined-cycle gas turbine (CCGT) plants, which integrate gas and steam cycles to achieve higher thermal efficiencies. Under favorable operating conditions, these plants can attain thermal efficiencies of approximately 60% [2], compared with values typically below 40% for conventional single-cycle gas turbine plants [3].

A combined-cycle gas turbine (CCGT) plant generates electricity by integrating two thermodynamic cycles: the Brayton cycle, in which a gas turbine operates, and the Rankine cycle, which utilizes the waste heat recovered from the gas turbine exhaust to produce steam and generate additional power. These plants are often designed with excess generating capacity to meet government-mandated reserve requirements [4]. However, fluctuations in electricity demand throughout the day may force CCGT plants to operate under off-design conditions, thereby reducing their thermal efficiency. Under such conditions, the mismatch between operating conditions and design specifications can lead to suboptimal energy utilization and increased energy losses [4].

Therefore, a thorough understanding of the thermodynamic behavior of CCGT plants is essential for the design and operation of more efficient power generation systems. Furthermore, thermodynamic modeling enables the simulation and evaluation of different operating scenarios, providing insights into system performance under varying operating conditions. In this context, accurate CCGT plant modeling is a valuable tool for optimizing fuel consumption, improving energy efficiency, and reducing fossil fuel use, thereby contributing to more sustainable electricity generation.

In the study by Yu et al. [5], a hybrid modeling approach that combines physical mechanisms with operational data to develop "gray-box" models of thermal systems is proposed. The key characteristics of the equipment are mapped from historical operational data, and the system models are built from mass and energy balances and thermodynamic equations. Additionally, Yu et al. [5] conducted a case study on a 660 MW double-reheat thermal power plant in operation. Moreover, Bishal et al. [6] describe a combined-cycle model with a supercritical CO_2 Brayton cycle as the topping cycle and an organic Rankine cycle as the bottoming cycle, developed in Python with the CoolProp library.

Building on the development of thermodynamic models, several studies have explored strategies to enhance the operational performance of combined-cycle gas turbine (CCGT) plants, particularly through supplementary firing in the heat recovery steam generator (HRSG). In the study by Lugo-Leyte et al. [7], a triple-pressure combined-cycle power plant operating with and without supplementary firing was analyzed to assess its effects on net power output, thermal efficiency, and exergy destruction. The results indicated that supplementary firing increased net power generation and improved heat recovery steam generator performance, but reduced the overall thermal efficiency of the combined cycle. However, the study focused exclusively on thermodynamic performance and did not assess the implications of supplementary firing for electricity generation costs.

Although thermodynamic analyses provide valuable information regarding plant performance, they do not quantify the economic consequences associated with thermodynamic irreversibilities. To address this limitation, Ahmadi et al. [8] incorporated exergoeconomic and environmental analyses into the optimization of combined-cycle power plants equipped with supplementary firing. Their work demonstrated the relevance of combining thermodynamic and economic criteria for plant assessment. However, the proposed

methodology focused on optimization and did not evaluate the component-by-component cost formation under different operating conditions using the SPECO methodology.

Among the available exergoeconomic approaches, the SPECO methodology, proposed by Lazzaretto and Tsatsaronis [9], has become one of the most widely adopted procedures for allocating exergy costs in thermal systems because of its systematic fuel-product formulation and component-based cost balances. Despite its extensive application to thermal systems, SPECO has mostly been applied to design-point or simulated operating conditions, and the studies that address supplementary firing either restrict the assessment to thermodynamic performance [7] or use exergoeconomic indicators as objective functions of an optimization procedure [8]. Consequently, the component-by-component cost formation of a real combined-cycle plant, evaluated from measured operating data and compared between operation with and without supplementary firing, remains insufficiently documented. This gap motivates the methodology proposed in the present work.

Therefore, this study develops a Python-based thermodynamic model of an isolated natural gas-fired combined-cycle power plant to perform integrated energy, exergy, and exergoeconomic analyses under operating conditions with and without supplementary firing.

The main contributions of this work are: (i) an open, Python-based model of a real plant configuration (two alternately operated gas turbines, a heat recovery steam generator with a screen, two superheaters, and a supplementary burner, and a single steam turbine), fed with operational data from the plant; (ii) a component-by-component application of the SPECO methodology that explicitly includes the supplementary burner and each HRSG heat exchanger, allowing the identification of where the electricity cost is formed; (iii) a direct comparison between operation with and without supplementary firing in terms of the distribution of exergy destruction and of the cost formation of electricity; and (iv) the evaluation of the specific exergy cost of electricity as a function of the gross electrical power over the actual operating range of the plant.

The proposed model, implemented in Python and validated against the measured steam production of the plant, provides a flexible and reproducible framework for evaluating the thermodynamic and exergoeconomic performance of CCGT systems.

2. Materials and Methods

2.1. Combined Cycle

A combined cycle integrates two power cycles so that the thermal energy rejected by the first cycle, which would otherwise be wasted, is partially or completely used by the second. In a gas–steam combined cycle, the two cycles are interconnected through a heat recovery steam generator (HRSG), which acts as the boiler of the steam cycle. The combination provides a high mean temperature of heat addition, in the Brayton cycle, and a low mean temperature of heat rejection, in the Rankine cycle, which results in a higher efficiency than that of each cycle individually [10].

2.2. Thermodynamic Analysis

Energy analysis evaluates the performance of systems that exchange energy as heat and work. It is based on the first law of thermodynamics, which states that the total energy of an isolated system remains constant; i.e., it expresses the principle of conservation of energy [10]. Energy analysis makes it possible to identify process bottlenecks, energy losses, and the efficiencies of individual components and of the entire plant, and this diagnosis guides the solution of operational problems, contributing to reducing financial losses and improving processes [3].

Although energy balances provide important information on the behavior of a system, they have limitations. For instance, energy analysis cannot identify the components in which the quality of energy is most degraded, that is, those with the largest irreversibilities. An irreversible process is one after which the system and its surroundings cannot both be restored exactly to their initial states [10].

Exergy analysis, based on the second law of thermodynamics, provides a more comprehensive understanding of the operation of the systems analyzed, allowing: (i) the prediction of process directions; (ii) the establishment of equilibrium conditions; (iii) the determination of the best theoretical performance of cycles, engines, and other devices; (iv) the quantitative evaluation of factors that prevent achieving the best theoretical performance; and (v) the creation of methods to evaluate enthalpy in terms of properties more easily obtained experimentally [10].

2.3. Methodology of the Study

This section describes the plant studied and its main components, the assumptions of the model, the combustion stoichiometry, and the energy, exergy, and exergoeconomic models of the plant. The properties of water and steam were obtained from the IAPWS-IF97 formulation [11], as implemented in the IAPWS Python package (version 1.5.5), and the model was implemented in Python 3.11.9 (Python Software Foundation, Beaverton, OR, USA). Air and exhaust gas were treated as ideal-gas mixtures of fixed composition, with the enthalpy and entropy of each species obtained from the NASA seven-coefficient polynomials of the GRI-Mech 3.0 thermodynamic database; the enthalpies of both mixtures are sensible enthalpies referred to 25 °C, so that air and exhaust gas share the same reference state.

2.3.1. Plant Description

Figure 1 shows the simplified thermodynamic diagram of the thermal power plant with each flow properly identified; the thermal generation system comprises a combined gas-steam cycle. This system includes two gas turbines and one steam turbine, with the gas cycles operating alternately. Thus, there is no simultaneous operation of the two Brayton cycles.

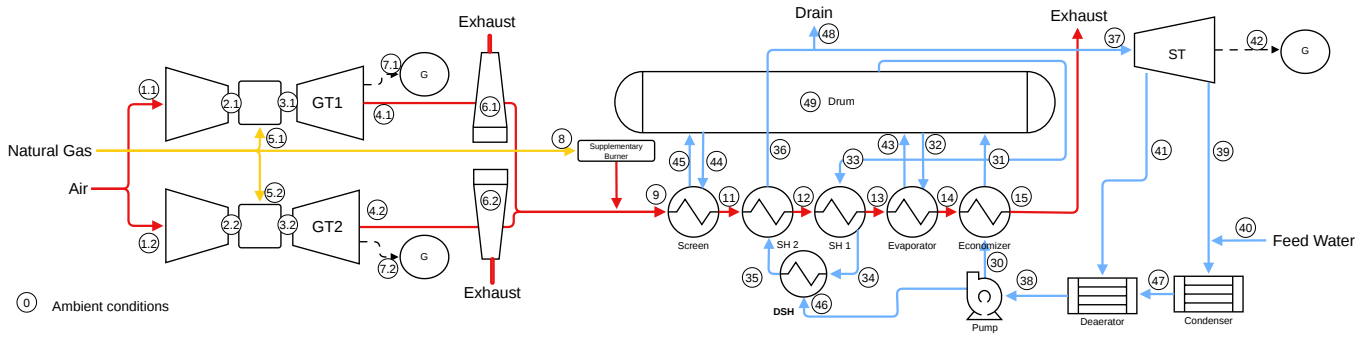


Figure 1. Thermodynamic diagram of the plant studied.

The gas turbine cycle comprises a compressor, a combustion chamber, a gas turbine (expander), and an electric generator. The overall efficiency of this unit ranges from 34.8% to 35.6%. The exhaust gas temperature varies between 510 and 555 °C, while the exhaust gas mass flow rate ranges from 34.2 to 44.5 kg/s.

The steam cycle features a turbine with a nominal power output of 12 MW, operating at pressures of up to 5800 kPa and temperatures of up to 497 °C. The steam turbine exhaust pressure reaches values as low as 7 kPa, and its rotational speed is 6800 rpm.

The heat recovery steam generator (HRSG) consists of a series of heat exchangers designed to recover thermal energy from the gas turbine exhaust and transfer it to the steam cycle. In the power plant investigated in this study, the HRSG comprises an economizer, an evaporator, a steam drum, two superheaters interconnected by a desuperheater, and a screen. Measures are required to prevent excessive temperatures in the second superheater, both to mitigate the risk of equipment damage and to control the steam turbine inlet temperature within the allowable limits imposed by the materials used in its construction. Accordingly, the HRSG considered in this study is equipped with a screen supplied with recirculating water, positioned at the exhaust gas inlet to regulate the thermal conditions within the heat recovery system [12].

Following the characterization of the thermoelectric power plant, relevant points throughout the system were selected for data collection, including pressure, temperature, and mass flow rate. The thermodynamic model of the plant was then developed from these operating data and from equipment specifications obtained from the literature.

2.3.2. Hypotheses and Considerations

The following simplifying assumptions, based on the literature, were adopted in the thermodynamic model:

- All components operate at steady state.
- Kinetic and potential energies were neglected.
- The dead state was defined according to ambient temperature and pressure measurements.
- Under these assumptions, the specific exergy of a state i is determined by Equation (1):

$$x_i = h_i - h_0 - T_0 \cdot (s_i - s_0) \quad (1)$$

- Equation (1) accounts only for the physical exergy of the air, exhaust gas, and water streams, whereas the fuel enters the system with its chemical exergy (Equation (2)). The chemical exergy of the combustion products, associated with the difference between their composition and that of the reference environment [13], was neglected. Using the exhaust gas composition adopted below, this term is approximately 16 kJ/kg, i.e., about 0.62 MW for the exhaust gas flow rate at the representative operating point (Section 3.2), compared with about 0.04 MW for the inlet air. Its inclusion would reduce the exergy destruction rate of the combustion chamber by about 0.64 MW (≈5%) and that of the supplementary burner by about 0.25 MW (≈7%). Since this exergy is not used in the downstream components and leaves the plant with the stack gases (state 15), it would be reclassified as an exergy loss rather than destruction, without changing the cycle exergy efficiency (Equation (28)) or the ranking of the components.
- A constant lower heating value (LHV) of 47.13 MJ/kg was adopted, according to [14]; this is the reference value used by the plant supervisory system to record the heat inputs of the combustion chamber and the supplementary burner (Section 2.3.3).
- The composition of the exhaust gases was considered as consisting of 74.12% N_2, 15.51% O_2, 4.88% CO_2, and 5.49% H_2O on a mass basis, for operation both with and without supplementary firing. As shown in Section 2.3.3, this composition differs from that calculated for the combustion chamber outlet by less than 0.5 percentage point, and their mean specific heats between 400 and 800 K, estimated from ideal-gas enthalpies [10], differ by 0.3%. After the supplementary burner, the O_2 content decreases and the mean specific heat is 0.6% higher than that of the adopted composition. Since N_2 accounts for about 74% of the mixture in all cases, the effect of this assumption on the energy and exergy balances of the HRSG is below 1%.
- The composition of the air was assumed to consist of 75.4% N_2, 23% O_2, and 1.6% H_2O.

- The molar mass considered was 28.0134 kg/kmol for N_2, 31.9988 kg/kmol for O_2, 44.0095 kg/kmol for CO_2, and 18.01528 kg/kmol for H_2O [15].
- The specific exergy of natural gas is obtained from Equation (2), where ϕ is the ratio of the chemical exergy of the fuel to its LHV. ϕ = 1.045 was adopted [16].

$$x_{\text{Fuel}} = \text{LHV} \cdot \phi \tag{2}$$

- The exergy of work is considered equal to the work itself, whether mechanical or electrical.

2.3.3. Combustion Stoichiometry

Natural gas is represented by an equivalent formula $C_xH_yO_zN_w$, obtained from its molar composition. The humid air defined in the previous section contains, per kmol of O_2, $b = 3.745$ kmol of N_2 and $c = 0.124$ kmol of H_2O. Assuming complete combustion without dissociation, the global reaction in the combustion chamber is given by Equation (3), where λ is the excess air ratio and a_{st} is the stoichiometric oxygen requirement, given by Equation (4).

$$\begin{aligned} C_xH_yO_zN_w + \lambda a_{\text{st}}(O_2 + b\,N_2 + c\,H_2O) \rightarrow x\,CO_2 + \left(\frac{y}{2} + \lambda a_{\text{st}} c\right)H_2O \\ + (\lambda - 1)\,a_{\text{st}}\,O_2 + \left(\lambda a_{\text{st}} b + \frac{w}{2}\right)N_2 \end{aligned} \tag{3}$$

$$a_{\text{st}} = x + \frac{y}{4} - \frac{z}{2} \tag{4}$$

The stoichiometric air–fuel ratio on a mass basis, AFR_{st}, and the excess air ratio of the combustion chamber, λ_{CC}, are given by Equations (5) and (6), where M denotes the molar mass and $\dot{m}_{\text{Air}}$ and $\dot{m}_{\text{NG,CC}}$ are the mass flow rates of air and natural gas in the gas turbine. The air flow rate is obtained as described in Section 2.3.4, and the natural gas flow rate as explained below.

$$\text{AFR}_{\text{st}} = \frac{a_{\text{st}}\left(M_{O_2} + b\,M_{N_2} + c\,M_{H_2O}\right)}{M_{\text{NG}}} \tag{5}$$

$$\lambda_{\text{CC}} = \frac{\dot{m}_{\text{Air}}/\dot{m}_{\text{NG,CC}}}{\text{AFR}_{\text{st}}} \tag{6}$$

The composition of the natural gas supplied to the plant was taken from the plant gas chromatograph and is given in Table 1. The heavier hydrocarbons are reported by the chromatograph as a single fraction, here represented by n-hexane. This composition corresponds to the equivalent formula $C_{1.304}H_{4.358}O_{0.003}N_{0.243}$, with a molar mass of 23.50 kg/kmol, $a_{\text{st}} = 2.392$ kmol of O_2 per kmol of fuel, and $\text{AFR}_{\text{st}} = 14.16$ kg of humid air per kg of fuel. The ratio of the chemical exergy to the LHV of this composition, calculated with the standard chemical exergies of its components [13], is about 1.04, consistent with the value of $\phi = 1.045$ adopted in this study.

Table 1. Composition of the natural gas measured by the plant gas chromatograph (molar fractions, %).

CH_4	C_2H_6	C_6H_{14}	N_2	CO_2	C_3–C_5
72.08	8.90	6.72	12.13	0.17	0.00

The LHV of 47.13 MJ/kg adopted in the model is the reference value used by the plant supervisory system to record the heat inputs of the combustion chamber and the supplementary burner. Since these heat inputs are taken directly from the plant records,

the energy and exergy balances of the model depend essentially on the recorded heat input, and the fuel exergy is obtained as $\dot{Q}\,\phi$; the LHV only affects the natural gas mass flow rate, which represents about 2% of the exhaust gas flow rate. For the stoichiometric analysis, the natural gas flow rates were obtained by dividing the recorded heat inputs by the LHV of the measured composition, calculated with the heating values of its components [17], $\dot{m}_{NG} = \dot{Q}/\mathrm{LHV}$, so that the mass of fuel is consistent with its composition.

At the operating point of Section 3.2, the air and natural gas flow rates (39.02 and 0.855 kg/s) correspond to an air–fuel ratio of 45.6 and $\lambda_{CC} = 3.22$, i.e., about 220% excess air. Over the analyzed period, the median excess air ratio was 3.29 (interquartile range 3.25–3.37). This large excess of air, typical of gas turbines, limits the turbine inlet temperature and supports the assumption of complete combustion.

The supplementary burner burns natural gas with the oxygen remaining in the exhaust gas, without additional air. Its products are obtained from Equation (3) with the total fuel flow rate, $\dot{m}_{NG,CC} + \dot{m}_{NG,SB}$, and the overall excess air ratio after the burner is $\lambda_{SB} = [\dot{m}_{Air}/(\dot{m}_{NG,CC} + \dot{m}_{NG,SB})]/\mathrm{AFR}_{st}$. At the representative operating point, $\lambda_{SB} = 2.56$; with the burner on, its median value in the period was 2.96 and its minimum was 2.56, so the oxygen available in the exhaust gas was always sufficient for complete combustion. The calculated compositions of the combustion products are compared with the exhaust gas composition adopted in the model in Table 2.

Table 2. Composition of the combustion products at the representative operating point, calculated with Equation (3), and exhaust gas composition adopted in the model (mass fractions, %).

Stream	λ	N_2	O_2	CO_2	H_2O
Combustion chamber outlet (state 3)	3.22	74.09	15.52	5.24	5.15
Supplementary burner outlet (state 11)	2.56	73.76	13.64	6.56	6.04
Adopted composition	–	74.12	15.51	4.88	5.49

2.3.4. Energy Model

Energy balances based on the first law of thermodynamics were applied to each component of the diagram (Table 3). The mass flow rate $\dot{m}$, temperature T, and pressure p define the thermodynamic states of the working fluids, from which the specific enthalpy h, specific entropy s, and quality q, as well as the performance parameters of the components, are calculated.

The resulting equations are Equations (7)–(15). In these equations, all work rates are expressed as positive magnitudes: $\dot{W}_{Comp}$ is the power consumed by the compressor, and $\dot{W}_{GT}$ and $\dot{W}_{ST}$ are the power produced by the gas and steam turbines.

The combustion process is modeled as a heat addition to the working fluid. The heat input of the combustion chamber, $\dot{Q}_{CC}$, was obtained from the heat rate of the gas turbine recorded by the plant at each instant, and the natural gas mass flow rate, $\dot{m}_{NG,CC}$, was determined from Equation (9) using the constant LHV. The mass balance of the combustion chamber is given by Equation (8). Since the enthalpies of air and exhaust gas share the same reference state, the energy balance of the adiabatic chamber is $\dot{m}_{EG}h_3 = \dot{m}_{Air}h_2 + \dot{Q}_{CC}$. The air mass flow rate and the turbine inlet temperature (state 3) are not measured. They are obtained by solving this energy balance together with the power balance of the gas turbine shaft, $\dot{W}_{GT} - \dot{W}_{Comp} = \dot{W}_{7e}/\eta_{gen,GT}$, where $\dot{W}_{7e}$ is the measured electrical power of the GT generator and $\eta_{gen,GT} = 0.97$. The temperatures at states 1, 2, and 4 are measured, and the compressor outlet and turbine inlet pressures were taken as 1676 and 1642 kPa.

Table 3. Equations of the energy model.

Component	Equation	
Compressor	$\dot{W}_{\text{Comp}} = \dot{m}_{\text{Air}} \cdot (h_2 - h_1)$	(7)
Combustion Chamber	$\dot{m}_{\text{EG}} = \dot{m}_{\text{Air}} + \dot{m}_{\text{NG,CC}}$	(8)
	$\dot{Q}_{\text{CC}} = \dot{m}_{\text{NG,CC}} \cdot \text{LHV}$	(9)
Gas Turbine	$\dot{W}_{\text{GT}} = \dot{m}_{\text{EG}} \cdot (h_3 - h_4)$	(10)
Supplementary Burner	$\dot{m}_{11} = \dot{m}_{10} + \dot{m}_{\text{NG,SB}}$	(11)
	$\dot{Q}_{\text{SB}} = \dot{m}_{\text{NG,SB}} \cdot \text{LHV}$	(12)
	$\dot{m}_{11} \cdot h_{11} = \dot{m}_{10} \cdot h_{10} + \dot{Q}_{\text{SB}}$	(13)
HRSG (each heat exchanger)	$\dot{m}_{\text{Water,out}} \cdot h_{\text{Water,out}} - \dot{m}_{\text{Water,in}} \cdot h_{\text{Water,in}} = \dot{m}_{\text{EG,in}} \cdot h_{\text{EG,in}} - \dot{m}_{\text{EG,out}} \cdot h_{\text{EG,out}}$	(14)
Steam Turbine	$\dot{W}_{\text{ST}} = \dot{m}_{37} \cdot (h_{37} - h_{39})$	(15)

At the operating point of Section 3.2, $\dot{Q}_{\text{CC}} = 35.17$ MW. This corresponds to a heat rate of about 10 420 kJ/kWh and to a gas cycle efficiency of 34.5%, close to the nominal range of the gas turbine set (34.8–35.6%). The resulting natural gas and air flow rates are 0.746 and 39.02 kg/s, respectively, the latter within the nominal range of Section 2.3.1. Complete combustion is assumed, and dissociation is neglected, which is consistent with the large excess of air (Section 2.3.3). The supplementary burner is also modeled as an adiabatic heat addition, with the heat input recorded by the plant, $\dot{Q}_{\text{SB}}$, from which its natural gas flow rate, $\dot{m}_{\text{NG,SB}}$, is obtained (Equations (11)–(13)). The duct between the gas turbine and the burner (states 4 and 10) is considered without losses.

The total heat input of the plant is the sum of the heat inputs of the combustion chamber and the supplementary burner, $\dot{Q}_{\text{in}} = \dot{Q}_{\text{CC}} + \dot{Q}_{\text{SB}} = (\dot{m}_{\text{NG,CC}} + \dot{m}_{\text{NG,SB}})\,\text{LHV}$. The gross electrical power of the plant, $\dot{W}_{\text{gross}} = \dot{W}_{7e} + \dot{W}_{42e}$, is the sum of the measured electrical power of the GT and ST generators. The net electrical power, $\dot{W}_{\text{net}} = \dot{W}_{\text{gross}} - \dot{W}_{\text{aux}}$, discounts the auxiliary consumption of the plant, $\dot{W}_{\text{aux}}$, obtained as the difference between the gross and net power recorded by the substation meter. This record was available and consistent with the generator measurements (deviation below 5%) in 720 of the 1027 operating points analyzed; in these points, the auxiliary consumption had a median of 3.2% of the gross power (interquartile range 2.7–3.7%). The efficiencies and costs presented in Section 3 refer to the gross power, unless otherwise stated, and the corresponding net values are given for comparison.

In the HRSG, the flow rates, pressures, and temperatures of the feedwater and steam (states 30 to 37) are measured, as is the stack gas temperature (state 15). The exhaust gas temperatures between the heat exchangers (states 14, 13, 12, and 9) are obtained from the energy balances of the economizer, evaporator, superheater 1, and superheater 2 (Equation (14)), assuming adiabatic heat exchangers. These balances proceed from the stack towards the HRSG inlet. Therefore, the difference between the heat released by the exhaust gas and the heat absorbed by the water in the whole HRSG is attributed to the screen.

The heat of evaporation (from state 31 to saturated steam, state 33) is divided between the screen and the evaporator. The division is proportional to the heat released by the exhaust gas in each section, estimated from the measured gas temperatures at states 9, 13,

and 14. The recirculation flow rates of the screen and evaporator are not measured. For this reason, the product of each of these components is the exergy of the heat absorbed at the saturation temperature, $\dot{Q}(1 - T_0/T_{sat})$. When the measured economizer outlet temperature reaches saturation, as occurs during operation without supplementary firing, state 31 is taken as saturated liquid.

The steam extraction of the steam turbine (state 41 in Figure 1) was closed during the analyzed period (measured flow rate close to zero); therefore, the whole steam flow rate expands from state 37 to state 39 in Equation (15). The enthalpy at the turbine outlet (state 39) is obtained from the measured electrical power of the ST generator, with $\eta_{gen,ST} = 0.90$. The isentropic efficiencies of the compressor and turbines are given by Equations (16)–(18), where the subscript s denotes the state reached at the same outlet pressure by an isentropic process. The first-law efficiency of the combined cycle is given by Equation (19) on gross and net bases, and that of the gas cycle alone is $\eta_{I,GC} = \dot{W}_{7e}/\dot{Q}_{CC}$.

$$\eta_{I-Comp,s} = \frac{(h_{2,s} - h_1)}{(h_2 - h_1)} \tag{16}$$

$$\eta_{I-GT,s} = \frac{(h_3 - h_4)}{(h_3 - h_{4,s})} \tag{17}$$

$$\eta_{I-ST,s} = \frac{(h_{37} - h_{39})}{(h_{37} - h_{39,s})} \tag{18}$$

$$\eta_{I,gross} = \frac{\dot{W}_{7e} + \dot{W}_{42e}}{\dot{Q}_{CC} + \dot{Q}_{SB}}, \qquad \eta_{I,net} = \frac{\dot{W}_{gross} - \dot{W}_{aux}}{\dot{Q}_{CC} + \dot{Q}_{SB}} \tag{19}$$

2.3.5. Exergy Model

Exergy balances were likewise applied to each component (Table 4, Equations (20)–(24)). The specific enthalpy and entropy of each state give its specific exergy, x (Equation (1)), and the exergy rate of the stream, $\dot{X} = \dot{m}x$. Throughout this paper, $\dot{X}$ denotes the exergy rate of a stream, whereas $\dot{E}_F$, $\dot{E}_P$, and $\dot{E}_D$ denote the fuel, product, and destruction exergy rates of a component.

Table 4. Equations of the exergy model.

Component	Equation	
Compressor	$\dot{X}_{in} + \dot{W}_{Comp} = \dot{X}_{out} + \dot{E}_{D,Comp}$	(20)
Combustion Chamber	$\dot{X}_{in} + \dot{X}_{NG} = \dot{X}_{out} + \dot{E}_{D,CC}$	(21)
Gas Turbine	$\dot{X}_{in} = \dot{X}_{out} + \dot{W}_{GT} + \dot{E}_{D,GT}$	(22)
HRSG (each heat exchanger)	$\dot{X}_{EG,in} + \dot{X}_{Water,in} = \dot{X}_{EG,out} + \dot{X}_{Water,out} + \dot{E}_{D,HX}$	(23)
Steam Turbine	$\dot{X}_{in} = \dot{X}_{out} + \dot{W}_{ST} + \dot{E}_{D,ST}$	(24)

As explained in [10], Equation (25) refers to the second-law efficiency for devices that produce work, such as expansion turbines, while Equation (26) represents this efficiency for equipment that consumes work, such as compressors and pumps. Equation (27) applies to heat exchangers without mixing of the fluids, such as the HRSG components described in Section 2.3.1. Equation (28) gives the exergy efficiency of the combined cycle on gross and

net bases: the product is the electrical power, and the fuel is the exergy of the natural gas consumed in the combustion chamber and in the supplementary burner (states 5 and 8). For the gas cycle alone, $\eta_{\mathrm{II,GC}} = \dot{W}_{7e}/\dot{X}_5$. For the combustion chamber and the supplementary burner, the exergy efficiency is defined as the ratio between the exergy increase of the gas stream and the exergy of the natural gas consumed, $\eta_{\mathrm{II-CC}} = (\dot{X}_3 - \dot{X}_2)/\dot{X}_5$ and $\eta_{\mathrm{II-SB}} = (\dot{X}_{11} - \dot{X}_{10})/\dot{X}_8$, consistent with the fuel and product definitions of Table 5; the exergy destruction rate of the combustion chamber is obtained from Equation (21) as $\dot{E}_{\mathrm{D,CC}} = \dot{X}_2 + \dot{X}_5 - \dot{X}_3$.

$$\eta_{\mathrm{II-W,out}} = \frac{w_{\mathrm{T}}}{x_{\mathrm{in}} - x_{\mathrm{out}}} \tag{25}$$

$$\eta_{\mathrm{II-W,in}} = \frac{x_{\mathrm{in}} - x_{\mathrm{out}}}{w_{\mathrm{Comp}}} \tag{26}$$

$$\eta_{\mathrm{II-Q}} = \frac{\dot{m}_{\mathrm{Water}} \cdot (x_{\mathrm{Water,out}} - x_{\mathrm{Water,in}})}{\dot{m}_{\mathrm{EG,out}} \cdot (x_{\mathrm{EG,in}} - x_{\mathrm{EG,out}})} \tag{27}$$

$$\eta_{\mathrm{II,gross}} = \frac{\dot{W}_{7e} + \dot{W}_{42e}}{\dot{X}_5 + \dot{X}_8}, \qquad \eta_{\mathrm{II,net}} = \frac{\dot{W}_{\mathrm{gross}} - \dot{W}_{\mathrm{aux}}}{\dot{X}_5 + \dot{X}_8} \tag{28}$$

Table 5. Fuel and product definitions of the plant components (states of Figure 1).

Component	$\dot{E}_{\mathbf{F}}$	$\dot{E}_{\mathbf{P}}$
Compressor	$\dot{W}_{3w}$	$\dot{X}_2 - \dot{X}_1$
Combustion chamber	$\dot{X}_5$	$\dot{X}_3 - \dot{X}_2$
Gas turbine	$\dot{X}_3 - \dot{X}_4$	$\dot{W}_{7w}$
GT generator	$\dot{W}_{7w} - \dot{W}_{3w}$	$\dot{W}_{7e}$
Supplementary burner	$\dot{X}_8$	$\dot{X}_{11} - \dot{X}_{10}$
Screen	$\dot{X}_{11} - \dot{X}_9$	$\dot{Q}_{\mathrm{scr}}(1 - T_0/T_{\mathrm{sat}})$
Superheater 2	$\dot{X}_9 - \dot{X}_{12}$	$\dot{X}_{36} - \dot{X}_{35}$
Superheater 1	$\dot{X}_{12} - \dot{X}_{13}$	$\dot{X}_{34} - \dot{X}_{33}$
Evaporator	$\dot{X}_{13} - \dot{X}_{14}$	$\dot{Q}_{\mathrm{ev}}(1 - T_0/T_{\mathrm{sat}})$
Economizer	$\dot{X}_{14} - \dot{X}_{15}$	$\dot{X}_{31} - \dot{X}_{30}$
Steam turbine	$\dot{X}_{37} - \dot{X}_{39}$	$\dot{W}_{42w}$
ST generator	$\dot{W}_{42w}$	$\dot{W}_{42e}$

2.3.6. Exergoeconomic Analysis

Exergy analysis is a fundamental tool for quantifying the exergy losses that occur in each component of a system and for evaluating the reduction in exergy from its introduction as fuel to the final generation of electricity. However, not all exergy losses have the same economic significance. Exergy losses occurring in downstream components, such as the generator, generally lead to higher economic penalties than those occurring in upstream components, such as the combustion chamber. This is because the exergy reaching the generator has already undergone several transformation processes and has accumulated the costs associated with all preceding stages. These costs are expressed in terms of the specific exergy cost, c (\$/GJ), which represents the cost per unit of exergy.

The specific exergy cost is determined using exergoeconomic balance equations, which account for the resources consumed and the useful products generated by each component of the system. The resources include the exergy associated with inlet streams, work and heat supplied to the component, fuel and electricity costs, and the equipment cost rate, which accounts for capital investment, installation, and maintenance expenses. The products are defined as the useful outputs of each component, which may include exergy streams, shaft work, electricity, or heat. By establishing the relationship between the resources

consumed and the products generated, the exergoeconomic balance equations enable the determination of the specific exergy cost associated with each output.

Once the specific exergy costs are determined, it becomes possible to identify cases in which reducing exergy destruction in components with higher exergy costs may be economically more effective, even if these components are not the largest contributors to exergy destruction.

Exergoeconomic Balance

The exergoeconomic balance of a component is described by Equation (29), which relates the costs associated with inlet and outlet exergy streams, heat transfer, work, and the component cost rate.

$$\sum c_{\text{in}} \dot{X}_{\text{in}} + \dot{Z} + c_{\text{Q}} \dot{E}_{\text{Q}} = \sum c_{\text{out}} \dot{X}_{\text{out}} + c_{\text{W}} \dot{W}, \tag{29}$$

where c is the specific exergy cost (\$/J). The subscripts *in*, *out*, *W*, and *Q* denote inlet streams, outlet streams, work, and heat transfer, respectively, and $\dot{E}_{\text{Q}}$ is the exergy transfer associated with heat transfer. For improved readability, the results are presented in \$/GJ by multiplying the values of c by 10^9. The term $\dot{Z}$ represents the component cost rate (\$/s).

In Equation (29), $\dot{E}_{\text{Q}}$ is considered positive when heat is supplied to the system, whereas $\dot{W}$ is considered positive when work is produced by the system. When the component rejects heat or consumes work, the corresponding terms may change sign or be transferred to the opposite side of the equation.

The cost associated with an exergy stream can also be expressed on a time basis as an absolute cost rate, $\dot{C}$ (\$/s), defined by Equation (30).

$$\dot{C} = c\dot{X}. \tag{30}$$

Fuel and Product Costs

Two parameters commonly employed in exergoeconomic analysis are the specific fuel cost, c_{F}, and the specific product cost, c_{P}, both expressed in \$/GJ. In the SPECO methodology [9], the fuel (F) of a component represents the exergetic resources expended to generate its product (P), both defined according to the purpose of the component. The F and P definitions adopted for each component are listed in Table 5. The specific fuel and product costs are then calculated with Equations (31) and (32), where $\dot{C}_{\text{F}}$ and $\dot{C}_{\text{P}}$ are the cost rates associated with the fuel and product exergy rates, $\dot{E}_{\text{F}}$ and $\dot{E}_{\text{P}}$. For each component, the cost balance of Equation (29) results in $\dot{C}_{\text{P}} = \dot{C}_{\text{F}} + \dot{Z}$.

$$c_{\text{F}} = \frac{\dot{C}_{\text{F}}}{\dot{E}_{\text{F}}}, \tag{31}$$

$$c_{\text{P}} = \frac{\dot{C}_{\text{P}}}{\dot{E}_{\text{P}}}. \tag{32}$$

The cost balances of the twelve components are complemented by the auxiliary equations of the SPECO methodology. According to the F rule, a stream that only supplies exergy to a component keeps its specific cost: $c_3 = c_4 = c_{10}$ (gas turbine and duct), $c_{11} = c_9 = c_{12} = c_{13} = c_{14} = c_{15}$ (gas side of the HRSG), and $c_{36} = c_{37} = c_{39}$ (steam turbine). According to the P rule, the products of a component have the same specific cost: $c_{3\text{w}} = c_{7\text{w}}$ (shaft work of the gas turbine). The steam drum, to which no investment cost was assigned, is described by the cost balance $c_{31}\dot{X}_{31} + c_{\text{P,scr}}\dot{E}_{\text{P,scr}} + c_{\text{P,ev}}\dot{E}_{\text{P,ev}} = c_d\,(\dot{X}_{33} + \dot{X}_{\text{bd}})$, where c_d is the common specific cost of its outlet streams, the saturated steam (state 33) and the blowdown (bd). Since no water injection occurs in the desuperheater at the analyzed

operating point, $c_{34} = c_{35}$. The inlet air and feedwater are taken with zero cost, and the natural gas streams (states 5 and 8) with the fuel price. The resulting system of 13 linear equations is solved simultaneously for each operating point.

Calculation of the Component Cost Rate

The component cost rate, $\dot{Z}$, is calculated using Equation (33), which accounts for the Purchase Equipment Cost (PEC), the Capital Recovery Factor (CRF), and a maintenance factor $\gamma = 1.06$ [8].

$$\dot{Z} = \frac{\mathrm{PEC} \cdot \mathrm{CRF} \cdot \gamma}{n_{\mathrm{h}} \cdot 3600}, \tag{33}$$

where the CRF (year^{-1}) is obtained from Equation (34). The CRF converts the investment into an equivalent annual cost over the plant lifetime, n_{years}, and the product $n_{\mathrm{h}} \cdot 3600$ converts this annual cost into a cost rate (\$/s). Therefore, the plant lifetime enters the calculation only through the CRF.

$$\mathrm{CRF} = \frac{i\,(1+i)^{n_{\mathrm{years}}}}{(1+i)^{n_{\mathrm{years}}} - 1}, \tag{34}$$

The values adopted in this study are:

- $n_{\mathrm{h}} = 8760$, annual operating hours;
- $n_{\mathrm{years}} = 20$, plant lifetime;
- $i = 12.4\%$, annual interest rate.

The maintenance factor γ accounts for the operation and maintenance costs as a fraction proportional to the investment cost [8]; it does not represent periods of unavailability of the plant. The annual operating time was taken as $n_{\mathrm{h}} = 8760$ h because the plant supplies an isolated system continuously and has two gas turbines operating alternately (Section 2.3.1), which allows the maintenance of one gas turbine while the other remains in operation. The symbol γ is used to distinguish the maintenance factor from the exergy-to-LHV ratio of the fuel, ϕ, defined in Equation (2).

Purchase Equipment Cost Correction

The PEC can be estimated either through a detailed economic model that accounts for equipment acquisition, installation, piping, instrumentation, and control costs, or by using literature values scaled to the capacity of the system under investigation. The latter approach was adopted in this study following the methodology proposed in [18–22], allowing direct comparison with previously published results.

The scaling of the reference cost, $\mathrm{PEC}_{\mathrm{ref}}$, is performed using Equation (35), where S is the capacity of the component, S_{ref} is the reference capacity, and α is the scaling exponent.

$$\mathrm{PEC}_{\mathrm{initial}} = \mathrm{PEC}_{\mathrm{ref}} \left(\frac{S}{S_{\mathrm{ref}}} \right)^{\alpha}, \tag{35}$$

The resulting value is then updated to the target year using the Chemical Engineering Plant Cost Index (CEPCI), as shown in Equation (36).

$$\mathrm{PEC}_{\mathrm{updated}} = \mathrm{PEC}_{\mathrm{initial}} \left(\frac{\mathrm{CEPCI}_{\mathrm{current}}}{\mathrm{CEPCI}_{\mathrm{initial}}} \right), \tag{36}$$

Finally, the PEC is obtained by applying the module factor F_{M}, according to Equation (37), where F_{M} is taken from [23].

$$\mathrm{PEC} = \mathrm{PEC}_{\mathrm{updated}} \cdot F_{\mathrm{M}}. \tag{37}$$

Relative Cost Difference and Exergoeconomic Factor

In this study, the SPECO methodology is used to assign specific costs to exergy streams and to calculate characteristic exergoeconomic indicators for each component. Let $c_{F,k}$ and $c_{P,k}$ denote the specific fuel and product costs of component k, respectively (\$/J). The relative cost difference, r_k, is defined by Equation (38). Positive values of r_k indicate that the cost per unit of exergy increases across the component, reflecting a significant economic impact on the final product cost, whereas negative values indicate a relative reduction in cost [24]. Since $\dot{C}_{P,k} = \dot{C}_{F,k} + \dot{Z}_k$, r_k can be written as $r_k = (1 - \eta_{ex,k})/\eta_{ex,k} + \dot{Z}_k/(c_{F,k}\dot{E}_{P,k})$, where $\eta_{ex,k} = \dot{E}_{P,k}/\dot{E}_{F,k}$ is the exergy efficiency of the component; the first term reflects the exergy destruction and the second the investment cost.

$$r_k = \frac{c_{P,k} - c_{F,k}}{c_{F,k}}. \tag{38}$$

In addition to r_k, the exergoeconomic factor, f_k, is used to assess the relative contribution of investment cost and exergy destruction cost to the total cost associated with component k. This parameter is defined by Equation (39), where $\dot{Z}_k$ is the capital cost rate and $\dot{C}_{D,k}$ is the cost rate associated with exergy destruction, $\dot{C}_{D,k} = c_{F,k}\dot{E}_{D,k}$. Values of f_k close to unity indicate that investment costs dominate, whereas low values indicate that exergy destruction costs are more significant [25].

$$f_k = \frac{\dot{Z}_k}{\dot{Z}_k + \dot{C}_{D,k}}. \tag{39}$$

Estimation of the Component Costs

The gas turbine and steam turbine units of the plant were acquired as integrated packages, and neither the purchase costs of their individual components nor the design data of the equipment (e.g., the heat transfer areas of the HRSG sections) are available. Therefore, the investment cost of each package was estimated, and the package cost was divided among its components using the cost structures reported in the literature for equipment of the same technology. The procedure comprises the following steps, and the values obtained in each step are summarized in Table 6. It should be emphasized that all the investment costs adopted in this study are academic estimates obtained from literature cost correlations and cost structures; they do not represent the actual purchase or contract costs of the plant equipment, and the exergoeconomic results should therefore be interpreted as estimates of the cost formation process.

1. Package costs: The PEC of the gas turbine package and of the steam turbine package was estimated with Equation (35), using the cost correlations of [23] for gas and steam turbines ("Motors, Drives" chart) and the reference values of [13,23,26]. The values were updated to the reference year with the CEPCI (Equation (36)) and corrected by the module factor (Equation (37)), resulting in 33.16 M\$ for the gas turbine package and 2.65 M\$ for the steam turbine package.
2. Gas turbine package: The package cost was divided among the GT generator (45%), gas turbine (25%), compressor (25%), and combustion chamber (5%), following the cost distribution reported by [27].
3. HRSG: The HRSG cost was taken as 11% of the gas turbine package cost, following [22], i.e., 3.65 M\$. This cost was divided among the supplementary burner, screen, superheaters, evaporator, and economizer in proportion to their heat transfer rates [18], as discussed below.
4. Steam turbine package: The ST generator was assigned 44.12% of the package cost, following [27], and the steam turbine the remaining 55.88%.

5. Cost rates: The cost rate of each component was calculated with Equation (33), with CRF = 0.1372 year^{-1} (i = 12.4% and n_{years} = 20), γ = 1.06, and n_{h} = 8760 h, so that each 1 M$ of PEC corresponds to 16.61 $/h.

Table 6. Estimation of the purchase equipment cost (PEC) and cost rate ($\dot{Z}$) of the plant components. The share is the fraction of the corresponding package (or HRSG) cost assigned to each component.

Package (Cost)	Component	Share (%)	PEC (M$)	$\dot{Z}$ ($/h)
Gas turbine (33.16 M$)	Compressor	25.0	8.29	137.68
	Combustion chamber	5.0	1.66	27.57
	Gas turbine	25.0	8.29	137.68
	GT generator	45.0	14.92	247.79
HRSG (3.65 M$)	Supplementary burner	13.5	0.49	8.20
	Screen	11.9	0.43	7.20
	Superheater 2	6.3	0.23	3.80
	Superheater 1	10.6	0.39	6.40
	Evaporator	30.0	1.10	18.21
	Economizer	27.7	1.01	16.81
Steam turbine (2.65 M$)	Steam turbine	55.88	1.48	24.58
	ST generator	44.12	1.17	19.43
Total			39.46	655.34

The HRSG cost was distributed among its six main components (supplementary burner, screen, superheater 2, superheater 1, evaporator, and economizer) in proportion to the heat transfer rate of each component, following [18]. This criterion was adopted because the purchase cost of the HRSG sections is mainly determined by their heat transfer area and, in the absence of geometric data for the HRSG, the heat transfer rate is the available indicator of the size of each section. It is a simplification, since it does not account for the differences in the overall heat transfer coefficient and in the mean temperature difference among the sections. Its effect on the results was assessed by repeating the calculations with the HRSG cost divided equally among the components and in proportion to their product exergy: the relative cost differences of the individual HRSG components changed (e.g., from 0.25 to 0.49 for superheater 2 and from 0.84 to 0.56 for the economizer), whereas the specific cost of electricity remained practically unchanged (13.97–13.98 $/GJ at the operating point of Section 3.2; Section 3.3), because the investment cost of the heat exchangers is entirely transferred to the steam regardless of how it is divided among them. No investment cost was assigned to the steam drum, whose outlet streams (saturated steam to superheater 1 and blowdown) receive the same specific cost, obtained from the cost balance between the drum inlet streams (water from the economizer and the products of the screen and evaporator) and outlet streams.

The cost shares of steps 2–4 distribute the investment cost of each package among its components, but they do not change the total investment cost of the plant. In the SPECO cost balances, all the costs that enter the plant (natural gas and $\sum \dot{Z}$) leave it either with the electricity or with the exergy losses (stack gas, steam turbine exhaust, and drum blowdown), and the latter are small: about 0.9 MW of the 46.3 MW of fuel exergy at the operating point of Section 3.2. Consequently, a different allocation within a package shifts costs among its components and between the electricity of the gas and steam turbines, changing the component-level indicators (r_k and f_k), but has only a small effect on the average specific cost of electricity of the plant. This behavior was confirmed for the HRSG, whose alternative cost allocations changed the electricity cost by less than 0.1% (Section 3.3). The allocation of the package costs is therefore a methodological simplification that affects

the indicators of the individual components within each package, but not the average cost of electricity. The uncertainty of the total investment cost, which directly affects the cost of electricity, was assessed by varying all PEC values by ±30% (Section 3.3).

The distribution of investment costs by system is shown in Figure 2. A constant natural gas price of 2.45 $/GJ was adopted, as reported by [18].

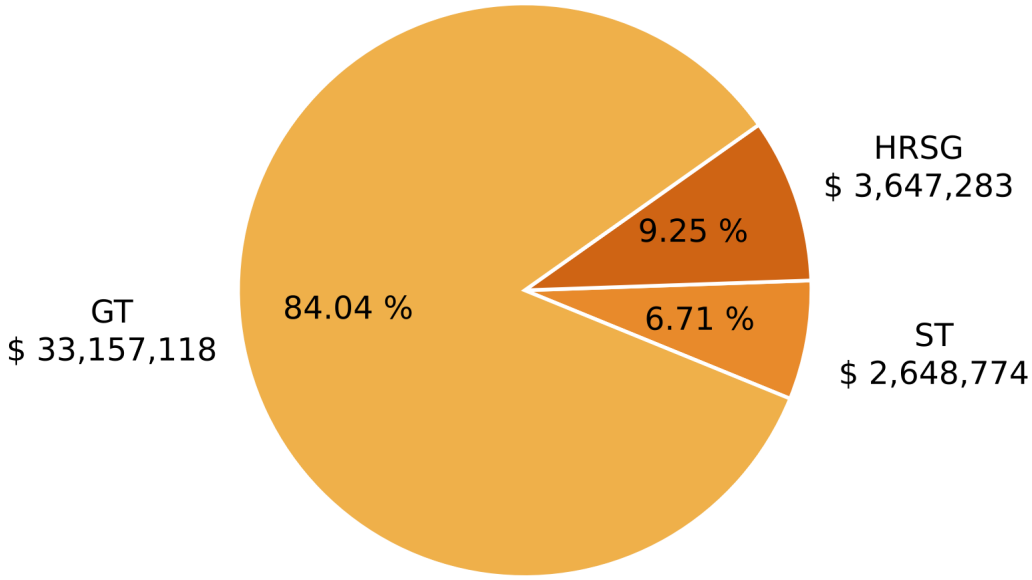


Figure 2. Distribution of investment costs by system.

3. Results and Discussion

This section presents the results of the energy, exergy, and exergoeconomic analyses of the plant.

The analyses use the 10-min records of the plant supervisory system for one month of operation (4464 records). Records with missing or inconsistent data were excluded, leaving 3073 records. Of these, 1190 correspond to combined-cycle operation (gas turbine above 5 MW and steam turbine above 2 MW).

To satisfy the steady-state assumption, only the records in which the electrical power of the gas turbine, the electrical power of the steam turbine, and the heat input of the supplementary burner varied by less than 0.5, 0.3, and 0.5 MW, respectively, with respect to the previous record were retained. The resulting 1027 operating points were simulated individually; in 620 of them the supplementary burner was off (heat input below 0.5 MW) and in 407 it was on. Since the distributions of several indicators are asymmetric, the results for the period are presented as medians, and the interquartile range is reported where relevant.

The results therefore represent the operation of the plant in the analyzed period and should be understood as a snapshot of the process in that time window. Changes in electricity demand, maintenance interventions, and the replacement or modification of equipment may alter the operating conditions and, consequently, the energy, exergy, and exergoeconomic indicators of the plant in other periods.

3.1. Model Validation

The electrical power of the gas and steam turbines, the heat input of the combustion chamber and the supplementary burner, and the water and steam conditions of the HRSG are inputs of the model, so they cannot be used to validate it. The validation was therefore based on variables that the model calculates and that are also measured at the plant.

The first is the steam mass flow rate: the exhaust gas flow rate is not measured and results from the energy balances of the gas turbine (Section 3.2); with it, the global energy balance of the HRSG between the supplementary burner outlet (state 11) and the stack (state 15) gives the steam mass flow rate that the exhaust gas can generate, which is compared with the measured steam flow rate (state 37). The second set comprises the exhaust gas temperatures between the HRSG sections (states 9, 13, and 14), calculated from the energy balances of the heat exchangers and compared with the measured values.

The comparison covers the 1027 operating points of the analyzed period and is shown in Figure 3 and Table 7, where the bias is the mean difference between calculated and measured values, RMSE is the root mean square error, MAPE is the mean absolute percentage error, and r is the Pearson correlation coefficient.

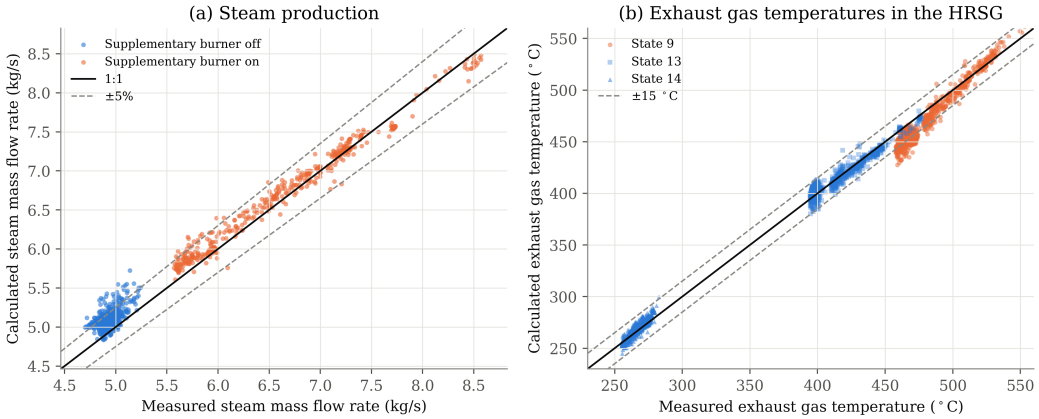


Figure 3. Calculated and measured values for the 1027 operating points of the analyzed period: (**a**) Steam mass flow rate; (**b**) exhaust gas temperatures between the HRSG sections.

Table 7. Deviation between calculated and measured values (analyzed period). SB: Supplementary burner.

SB	Variable	N	Measured	Calculated	Bias	RMSE	MAPE (%)	r
Off	$\dot{m}_{37}$ (kg/s)	620	4.92	5.09	+0.17	0.20	3.5	0.60
	T_9 (°C)		466.0	452.3	−13.7	14.7	2.9	0.48
	T_{13} (°C)		397.5	399.8	+2.3	5.4	1.1	0.29
	T_{14} (°C)		262.8	262.8	0.0	2.5	0.7	0.96
On	$\dot{m}_{37}$ (kg/s)	407	6.64	6.71	+0.07	0.14	1.8	0.99
	T_9 (°C)		508.3	506.7	−1.6	8.8	1.4	0.99
	T_{13} (°C)		431.7	429.7	−2.0	4.8	0.9	0.97
	T_{14} (°C)		266.0	269.9	+3.9	5.0	1.6	0.95
All	$\dot{m}_{37}$ (kg/s)	1027	5.60	5.74	+0.13	0.18	2.8	0.99
	T_9 (°C)		482.8	473.9	−8.9	12.7	2.3	0.99
	T_{13} (°C)		411.0	411.6	+0.6	5.2	1.0	0.97
	T_{14} (°C)		264.1	265.6	+1.5	3.7	1.0	0.94

The calculated steam flow rate deviates from the measured value by 2.8% on average (MAPE), with a correlation coefficient of 0.99 over the whole period. The model slightly overestimates the steam production (bias of +0.13 kg/s), which is consistent with the assumption of adiabatic heat exchangers, since the heat losses of the HRSG casing are not accounted for. The deviation is smaller with the supplementary burner on (1.8%) than off (3.5%). Without supplementary firing, the operating points are concentrated in a narrow range of steam flow rate (4.7–5.2 kg/s), which explains the lower correlation coefficient in this group despite the small absolute error (RMSE of 0.20 kg/s). The exhaust

gas temperatures at states 13 and 14 are reproduced with RMSE of about 5 °C. At state 9 (outlet of the screen), the model underestimates the temperature by 13.7 °C on average when the burner is off, because the heat released by the exhaust gas in the screen is obtained by difference and therefore accumulates the deviations of the other heat exchangers. The uncertainties of the plant instruments were not available and could not be propagated to the calculated results; therefore, the deviations in Table 7 include both model and measurement errors. Overall, the agreement indicates that the exhaust gas flow rate and the energy balances of the gas turbine and HRSG are consistent with the plant measurements.

3.2. Results at a Representative Operating Point

A representative operating point of the analyzed period was selected to present the detailed results. At this instant, the plant operated in steady state with the supplementary burner on: during the 90 min around this instant, the electrical power of the gas turbine (12.0–12.5 MW) and of the steam turbine (8.3–8.5 MW) and the heat input of the supplementary burner (8.8–9.1 MW) remained practically constant. The ambient temperature and pressure, which define the dead state, were 37.11 °C and 97.8 kPa. Table 8 summarizes the states considered for modeling. States 3*w*, 7*w*, and 42*w* represent shaft work: 3*w* is the work consumed by the compressor, 7*w* the work produced by the gas turbine, and 42*w* the work produced by the steam turbine.

States 7*e* and 42*e* represent the electrical power delivered by the GT and ST generators, which is the final product of the plant. The parameters q, h, and s were calculated by the energy model, while the exergy rate, $\dot{X}$, was derived from the exergy model. The specific exergy cost of each state, c, was obtained from the exergoeconomic model. The enthalpies of air and exhaust gas are sensible enthalpies referred to 25 °C. State bd represents the drum blowdown, and the recirculation states of the evaporator and screen (32, 43, 44, and 45 in Figure 1) and the extraction (41) are not required by the model (Section 2.3.1).

The parameters calculated for the main components are presented in Table 9. The exergy efficiency, η_{ex}, and the exergy destruction rate, $\dot{E}_D$, were obtained from the exergy model, whereas the component cost rate, $\dot{Z}$, the specific fuel and product costs, c_F and c_P, the relative cost difference, r_k, and the exergoeconomic factor, f_k, were determined using the exergoeconomic model.

To facilitate the interpretation of the exergy flow throughout the plant, a Sankey diagram was constructed for the same operating condition (Figure 4). The upper row represents the air and exhaust gas path, from the combustion chamber to the economizer, and the lower row represents the water and steam path, which receives the products of the HRSG heat exchangers and feeds the steam turbine; the arrows leaving each component upwards or downwards represent its exergy destruction, except for the electricity delivered by the generators and the exergy losses with the stack gases and in the condenser. For clarity, the water path is drawn following the horizontal position of the heat exchangers, so the intermediate values of this row do not correspond to physical states. At this operating point, the total natural gas mass flow rate was 0.94 kg/s, of which 20.6% was consumed in the supplementary burner. Of the 46.28 MW of fuel exergy, 20.61 MW (44.5%) were converted into electricity, 24.80 MW (53.6%) were destroyed in the components, and 0.90 MW (1.9%) left the plant as exergy losses with the stack gases, the steam turbine exhaust, and the drum blowdown.

Table 9 and Figure 4 show that the combustion chamber is the component with the highest exergy destruction rate, 12.40 MW (50% of the total), which reflects the strong irreversibilities associated with the combustion process and heat transfer under large temperature gradients. The supplementary burner presents the second highest exergy destruction

rate (3.60 MW) and an exergy efficiency of 0.62, similar to that of the combustion chamber (0.66), indicating that supplementary firing imposes a substantial thermodynamic penalty.

Table 8. Parameters of the main states in the diagram of Figure 1 (representative operating point). EG: Exhaust gas; NG: natural gas.

State	p (kPa)	T (°C)	$\dot{m}$ (kg/s)	q (–)	h (kJ/kg)	Fluid	s (kJ/kg K)	$\dot{X}$ (MW)	c ($/GJ)
1	98	14.07	39.02	-	-11.18	air	6.765	0.04	0.00
2	1676	423.29	39.02	-	419.98	air	6.867	15.63	11.98
3	1642	1125.55	39.77	-	1296.57	EG	7.820	39.98	7.12
4	100	529.76	39.77	-	558.41	EG	7.961	8.89	7.12
5	-	-	0.746	-	-	NG	-	36.76	2.45
3w	-	-	-	-	-	-	-	16.82	8.85
7w	-	-	-	-	-	-	-	29.35	8.85
7e	-	-	-	-	-	-	-	12.15	14.79
10	100	529.76	39.77	-	558.41	EG	7.961	8.89	7.12
8	-	-	0.193	-	-	NG	-	9.52	2.45
11	100	718.17	39.96	-	783.77	EG	8.213	14.81	6.00
9	100	590.17	39.96	-	629.63	EG	8.046	10.72	6.00
12	100	543.98	39.96	-	575.08	EG	7.981	9.34	6.00
13	100	473.89	39.96	-	493.49	EG	7.877	7.38	6.00
14	100	286.69	39.96	-	282.16	EG	7.552	2.96	6.00
15	100	127.12	39.96	-	108.59	EG	7.187	0.55	6.00
30	7530	55.20	8.75	-	237.48	water	0.767	0.08	0.00
31	4840	238.43	8.75	-	1030.23	water	2.684	1.82	10.56
33	4840	261.92	8.54	1.00	2795.52	water	5.988	8.09	9.49
34	4840	391.06	8.54	-	3177.53	water	6.634	9.64	9.38
35	4840	391.50	8.54	-	3178.61	water	6.635	9.64	9.38
36	4840	499.00	8.54	-	3433.98	water	6.992	10.88	9.17
37	4492	497.66	8.54	-	3434.86	water	7.026	10.80	9.17
39	8	42.26	8.54	0.90	2334.37	water	7.442	0.30	9.17
bd	4840	261.92	0.21	0.00	1144.37	water	2.902	0.05	-
42w	-	-	-	-	-	-	-	9.39	10.97
42e	-	-	-	-	-	-	-	8.46	12.81

Table 9. Parameters of the main components shown in Figure 1 (representative operating point).

Component	η_{ex}	$\dot{E}_D$ (MW)	$\dot{Z}$ ($/h)	c_F ($/GJ)	c_P ($/GJ)	r_k	f_k
Compressor	0.93	1.24	137.68	8.85	12.00	0.36	0.78
Combustion chamber	0.66	12.40	27.57	2.45	4.01	0.64	0.20
Gas turbine	0.94	1.73	137.68	7.12	8.85	0.24	0.76
GT generator	0.97	0.38	247.79	8.85	14.79	0.67	0.95
Supplementary burner	0.62	3.60	8.20	2.45	4.32	0.76	0.21
Screen	0.68	1.31	7.20	6.00	9.56	0.59	0.20
Superheater 2	0.90	0.14	3.80	6.00	7.53	0.25	0.56
Superheater 1	0.79	0.42	6.40	6.00	8.76	0.46	0.42
Evaporator	0.80	0.86	18.21	6.00	8.89	0.48	0.49
Economizer	0.72	0.68	16.81	6.00	11.07	0.84	0.53
Steam turbine	0.89	1.10	24.58	9.17	10.97	0.20	0.40
ST generator	0.90	0.93	19.43	10.97	12.81	0.17	0.35

Among the rotating components, the gas turbine exhibits the highest exergy efficiency (0.94), followed by the compressor (0.93) and the steam turbine (0.89). The HRSG heat exchangers present efficiencies ranging from 0.68 for the screen to 0.90 for superheater 2. Although the exergy destruction rates of the HRSG components are individually modest, their cumulative contribution (3.42 MW) is relevant to the overall plant performance.

The exergoeconomic results indicate that the GT generator has the highest component cost rate, with $\dot{Z} = 247.79$ \$/h, followed by the compressor and gas turbine, both with 137.68 \$/h. These values reflect the significant capital investment associated with the principal turbomachinery and electrical equipment.

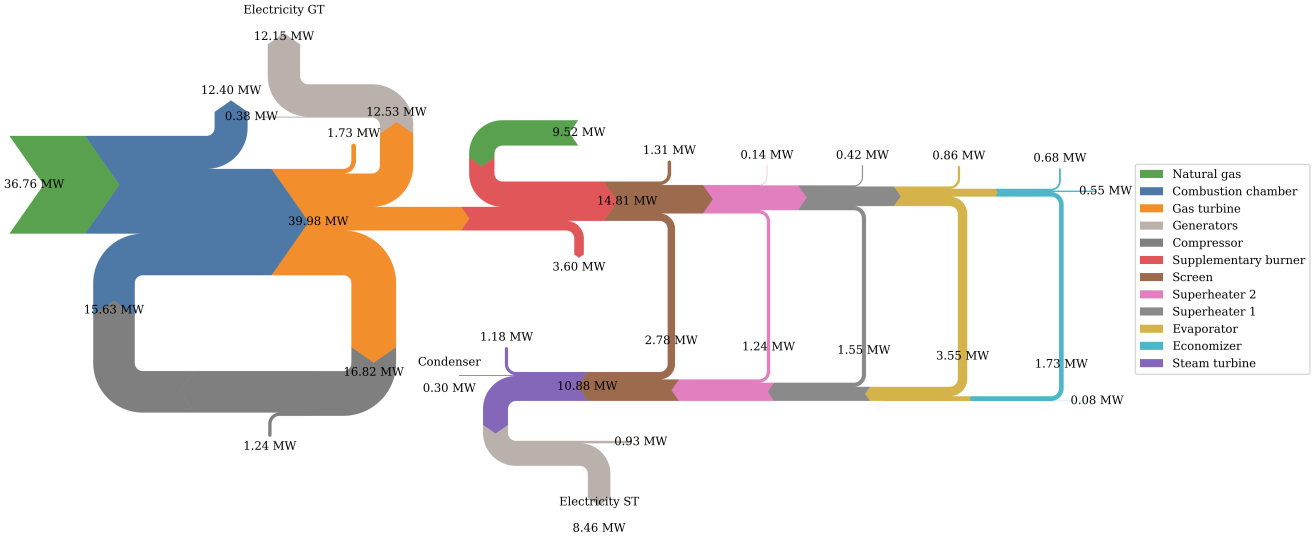


Figure 4. Exergy flow diagram at the representative operating point.

The specific cost increases across all components (Table 9). In the combustion chamber, it increases from 2.45 \$/GJ (natural gas) to 4.01 \$/GJ, and in the supplementary burner from 2.45 to 4.32 \$/GJ. At this operating point, the economizer presents the highest relative cost difference ($r_k = 0.84$): its exergy efficiency (0.72) accounts for 0.39 of this value, and its investment cost, which is high compared with the small exergy increase of the feedwater (1.74 MW), accounts for the remaining 0.45. The supplementary burner follows ($r_k = 0.76$); in this case, exergy destruction accounts for 0.61 of the value, because its product, the exergy increase of the exhaust gas (5.92 MW), is small compared with the fuel exergy it consumes (9.52 MW). The GT generator also presents a high value ($r_k = 0.67$), but its increase is due almost entirely to its investment cost, since its exergy destruction is small (0.38 MW). The combustion chamber presents $r_k = 0.64$: although it has the largest exergy destruction rate of the plant, its fuel is natural gas, the lowest-cost stream of the system, which limits the relative increase in specific cost. Nevertheless, the combustion chamber has by far the highest cost rate associated with exergy destruction, $\dot{C}_D = c_F \dot{E}_D \approx 109$ \$/h, followed by the gas turbine (44 \$/h) and the compressor (39 \$/h).

The exergoeconomic factor, f_k, provides insight into the relative importance of investment and exergy destruction costs. The GT generator has the highest value ($f_k = 0.95$), followed by the compressor ($f_k = 0.78$), the gas turbine ($f_k = 0.76$), superheater 2 ($f_k = 0.56$), and the economizer ($f_k = 0.53$), indicating that the total cost of these components is dominated by capital investment rather than thermodynamic inefficiencies. In contrast, the combustion chamber, the screen, and the supplementary burner present the lowest values ($f_k = 0.20$–0.21), showing that exergy destruction is the principal contributor to their overall cost. For these components, efforts to reduce irreversibilities are expected to be more economically effective than increasing capital expenditures.

Overall, the results demonstrate that the components with the largest thermodynamic inefficiencies are not necessarily those with the highest investment costs. The combustion chamber and the supplementary burner concentrate the exergy destruction and its cost, whereas the generators and turbomachinery are characterized by higher capital cost rates. This distinction highlights the importance of combining exergy and exergoeconomic

analyses to identify the components that offer the greatest potential for performance improvement and cost reduction. At this operating point, the specific exergy cost of the electricity produced by the GT and ST generators is 14.79 and 12.81 \$/GJ, respectively, corresponding to a weighted average of 13.98 \$/GJ. The electricity of the steam turbine is cheaper than that of the gas turbine at this instant because the high steam production obtained with supplementary firing distributes the investment cost of the steam cycle over a larger product. These costs refer to the gross electricity at the generator terminals. Since the auxiliary consumption (0.76 MW, 3.7% of the gross power at this instant) is supplied by the plant itself, the specific cost of the net electricity delivered to the isolated system is higher by the factor $\dot{W}_{\mathrm{gross}}/\dot{W}_{\mathrm{net}}$, i.e., 14.51 \$/GJ. At this operating point, the gross and net first-law efficiencies were 46.5% and 44.8%, and the corresponding second-law efficiencies were 44.5% and 42.9%.

3.3. Sensitivity of the Electricity Cost

The sensitivity of the specific cost of electricity to the main economic parameters was evaluated at the operating point of Section 3.2 by varying, one at a time, the natural gas price, the annual interest rate, and the annual operating time. The latter was reduced from 8760 h to 7884, 7008, and 6132 h, which correspond to availability factors of 90%, 80%, and 70%, respectively. To account for the uncertainty of the cost estimates, all purchase equipment costs were also varied by ±30%, and the two alternative distributions of the HRSG investment cost discussed in Section 2.3.6.6 were evaluated. The results are summarized in Table 10.

Table 10. Sensitivity of the specific exergy cost of electricity at the representative operating point. Base case: $c_{\mathrm{NG}} = 2.45$ \$/GJ, $i = 12.4\%$, and $n_{\mathrm{h}} = 8760$ h. The $\dot{Z}$ share is the fraction of the total cost rate (fuel plus $\sum \dot{Z}$) due to investment. SB: Supplementary burner.

Case	c_{elec} (\$/GJ)	Variation (%)	$\dot{Z}$ Share (%)	Highest r_k
Base case	13.98	—	61.6	Economizer (0.84)
$c_{\mathrm{NG}} = 1.23$ \$/GJ (−50%)	11.34	−18.9	76.3	Economizer (1.07)
$c_{\mathrm{NG}} = 3.68$ \$/GJ (+50%)	16.62	+18.9	51.7	Economizer (0.73)
$c_{\mathrm{NG}} = 4.90$ \$/GJ (+100%)	19.26	+37.8	44.5	SB (0.69)
$c_{\mathrm{NG}} = 7.35$ \$/GJ (+200%)	24.54	+75.6	34.9	SB (0.66)
$i = 8\%$	11.74	−16.0	54.4	Economizer (0.76)
$i = 10\%$	12.72	−9.0	57.9	Economizer (0.80)
$i = 14\%$	14.85	+6.2	63.8	Economizer (0.87)
$i = 16\%$	15.97	+14.2	66.4	Economizer (0.91)
$n_{\mathrm{h}} = 7884$ h (90%)	14.94	+6.9	64.1	Economizer (0.88)
$n_{\mathrm{h}} = 7008$ h (80%)	16.15	+15.6	66.7	Economizer (0.91)
$n_{\mathrm{h}} = 6132$ h (70%)	17.70	+26.7	69.6	Economizer (0.96)
PEC −30%	11.37	−18.7	52.9	Economizer (0.74)
PEC +30%	16.59	+18.7	67.6	Economizer (0.93)
HRSG cost: equal division	13.98	0.0	61.6	SB (0.80)
HRSG cost: product exergy	13.97	0.0	61.6	SB (1.02)

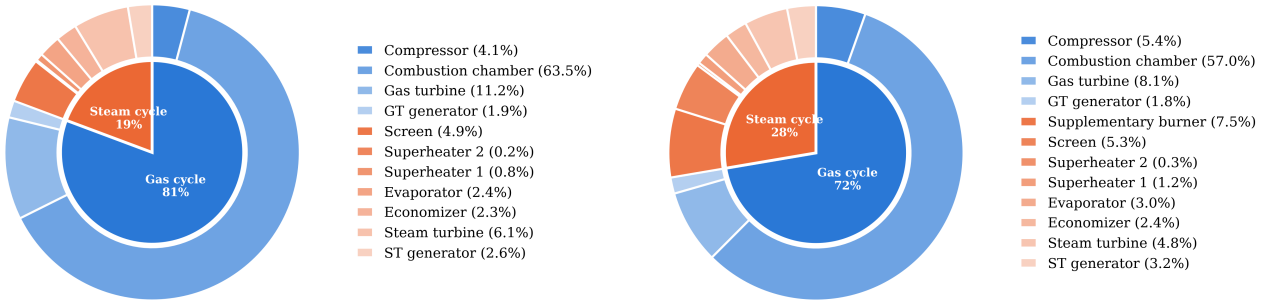
The specific cost of electricity varies linearly with the natural gas price, with a variation of ±18.9% for a ±50% change in the gas price, and increases by 6.9%, 15.6%, and 26.7% for availability factors of 90%, 80%, and 70%, respectively. Interest rates between 8% and 16% result in variations between −16.0% and +14.2%, while a ±30% variation in equipment purchase costs changes the electricity cost by ±18.7%. Since investment costs represent about 62% of the total cost in the base case, the electricity cost is sensitive to the economic

parameters affecting the investment cost rate. The distribution of the HRSG investment cost has a negligible effect on the electricity cost, which remains between 13.97 and 13.98 $/GJ, although it changes the indicators of individual HRSG components.

The main exergoeconomic conclusions remain consistent across the scenarios considered: the gas turbine, GT generator, and compressor remain dominated by investment costs ($f_k \geq 0.59$), whereas the combustion chamber, supplementary burner, and screen remain dominated by exergy destruction ($f_k \leq 0.40$). However, the component with the highest relative cost difference is not invariant. The economizer presents the highest value in the base case ($r_k = 0.84$), whereas the supplementary burner becomes the leading component at higher natural gas prices and under the alternative HRSG cost-allocation methods. These results indicate that, although the main distinction between investment-dominated and exergy-destruction-dominated components remains stable, the relative cost differences of individual components depend on the economic assumptions. Finally, since the sensitivity analysis was performed at a single representative operating point, further evaluation under different operating conditions would be necessary to determine whether these trends hold throughout the plant's operating range.

3.4. Exergy Destruction

To represent all the losses that occur in the system in relation to what is supplied, the percentage of exergy destruction is analyzed. The participation of each cycle (inner circle) and each piece of equipment (outer circle) in the mean exergy destruction rate of the plant in the analyzed period is shown in Figure 5a,b for the operating points with the supplementary burner off (620 points) and on (407 points), respectively. The mean exergy destruction rate was 17.10 MW with the burner off and 21.16 MW with the burner on.



(**a**) Supplementary burner off. (**b**) Supplementary burner on.

Figure 5. Mean share of the cycles and main components in the exergy destruction rate of the plant (analyzed period): (**a**) Supplementary burner off; (**b**) supplementary burner on.

The gas cycle accounts for 81% of the exergy destruction when the burner is off (Figure 5a) and 72% when the burner is on (Figure 5b). This is understandable because the gas cycle generates most of the electricity produced in the plant, about 72% of the total in the analyzed period. The decreasing order of the gas cycle equipment that destroys the most exergy remains the same for both scenarios: combustion chamber, gas turbine, compressor, and GT generator.

The steam cycle contributes 19% of the exergy destruction when the burner is off and 28% when the burner is on; most of this difference is due to the supplementary burner itself, which accounts for 7.5% of the total destruction when it is on.

A significant portion of the exergy supplied to the plant is destroyed in the components that first come into contact with natural gas: the combustion chamber (63.5% and 57% of the total in Figures 5a and 5b, respectively) and the supplementary burner (7.5% in Figure 5b).

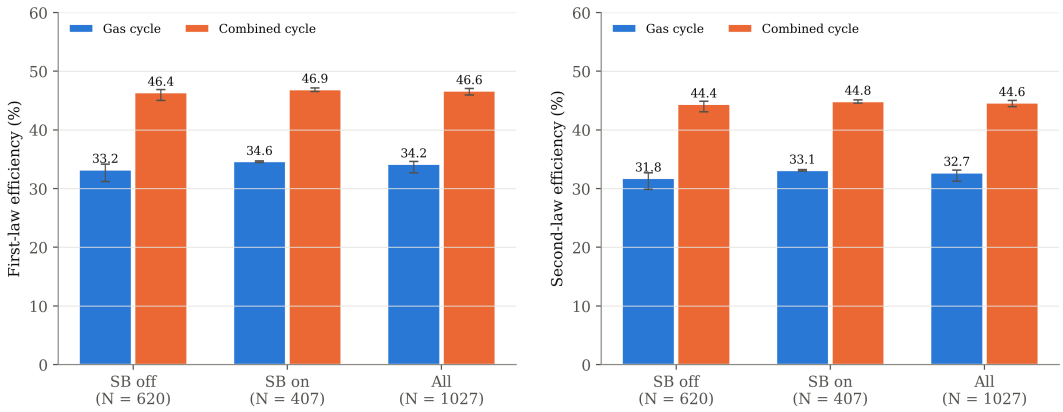
This result is consistent with the literature: in the 750 MW combined-cycle plant analyzed by Elwardany et al. [28], the combustion chambers account for 53.3% of the total exergy destruction.

For the scenario without supplementary firing, the decreasing order of the steam cycle equipment that destroys the most exergy is: steam turbine, screen, ST generator, evaporator, economizer, superheater 1, and superheater 2. With supplementary firing, the supplementary burner emerges first, followed by the screen, steam turbine, ST generator, evaporator, economizer, superheater 1, and superheater 2.

3.5. Energy and Exergy Efficiencies

Figure 6 shows the median first- and second-law efficiencies of the gas cycle (blue) and the combined cycle (orange) for the operating points with the supplementary burner off and on and for the whole period; the error bars indicate the interquartile range. The gas cycle, which generates most of the electricity, has a lower efficiency when considered alone (open cycle), because its exhaust gas leaves the turbine at high temperature (median of 528.5 °C in the analyzed period). Part of this energy is recovered in the HRSG to generate steam, which produces additional electricity in the steam cycle.

For the whole period, the gas cycle achieves a median first-law efficiency of 34.2% and the combined cycle 46.6% (gross basis, Equation (19)). As for the second-law efficiency (Equation (28)), the values are 32.7% and 44.6% for the same cycles. The combined-cycle efficiencies are slightly higher with the supplementary burner on (46.9% and 44.8%) than off (46.4% and 44.4%), mainly because the gas turbine operated at higher loads in these instants. When the auxiliary consumption is discounted, the median net first- and second-law efficiencies of the combined cycle are 45.1% and 43.2% (720 operating points with valid records of the auxiliary consumption), 44.9% and 43.0% with the burner off, and 45.3% and 43.4% with the burner on. These efficiencies are comparable to those reported for natural gas combined-cycle plants in operation. Bataineh and Khaleel [29] obtained energy and exergy efficiencies of 45.29% and 42.73% for a 430 MW combined-cycle plant in Jordan at an ambient temperature of 34 °C, similar to that of the plant studied here, and Elwardany et al. [28] reported 34.6% and 33.5% for a 750 MW combined-cycle plant in Egypt, while Ersayin and Ozgener [30] obtained 56% and 50.04% from the operational data of a combined-cycle plant. Therefore, although its capacity is much smaller (about 21 MW) and it operates in a hot climate, the plant studied presents a performance similar to that of large combined-cycle plants.



(**a**) First-law efficiency. (**b**) Second-law efficiency.

Figure 6. Median gross first- and second-law efficiencies of the gas cycle and of the combined cycle (analyzed period): (**a**) First-law efficiency; (**b**) second-law efficiency.

3.6. Specific Exergy Costs

The median specific exergy costs, c, of the principal thermodynamic states in the analyzed period are shown in ascending order in Figure 7, to illustrate the cost formation process throughout the plant. The first two states correspond to the compressor inlet air and the feedwater entering the HRSG, whose exergy costs were taken as zero.

The natural gas streams entering the combustion chamber and the supplementary burner (states 5 and 8) have the same specific exergy cost, equal to 2.45 $/GJ, which corresponds to the fuel price adopted in this study and constitutes the initial economic input to the system.

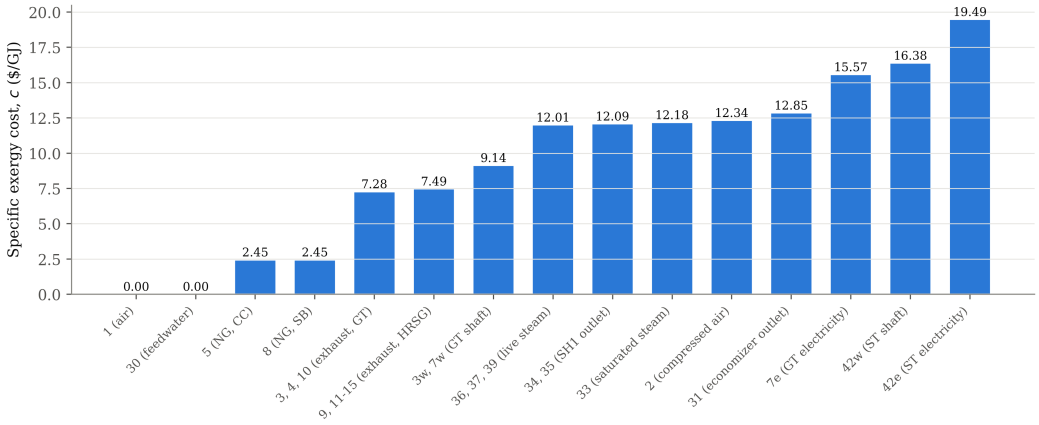


Figure 7. Median specific exergy cost of the principal thermodynamic states (analyzed period).

The exhaust gas leaving the gas turbine (states 3, 4, and 10) has a median specific exergy cost of 7.28 $/GJ. In the HRSG (states 9 and 11–15), the median is 7.49 $/GJ. When the supplementary burner is on, the cost of the exhaust gas decreases across the burner (from 7.08 to 6.67 $/GJ, medians of the operating points with the burner on), because the burner adds exergy at the cost of natural gas, which is lower than the cost of the exhaust gas. The water leaving the economizer (state 31) presents a median cost of 12.85 $/GJ, and the cost decreases slightly along the steam path, to 12.18 $/GJ for saturated steam (state 33) and 12.01 $/GJ for the live steam (states 36, 37, and 39), because the superheaters add exergy from the exhaust gas, whose cost is lower than that of the steam.

The shaft work of the gas turbine (states 3w and 7w) presents a specific exergy cost of 9.14 $/GJ, and the compressed air (state 2) reaches 12.34 $/GJ, which reflects the investment and exergy destruction costs of the compressor. The highest costs are those of the electricity generated by the GT and ST generators (states 7e and 42e), with medians of 15.57 and 19.49 $/GJ, respectively, and of the shaft work of the steam turbine (state 42w, 16.38 $/GJ).

For each component, the exergoeconomic balance establishes that the sum of the costs associated with all fuel streams, together with the component cost rate, $\dot{Z}$, must be equal to the cost of the product streams. This relationship allows the determination of the average specific fuel and product costs, denoted by c_F and c_P, respectively.

The median specific fuel and product costs of the modeled components are illustrated in Figure 8. The combustion chamber and the supplementary burner exhibit the lowest specific fuel cost, 2.45 $/GJ, because their fuel is natural gas, and their product costs are 4.02 and 5.05 $/GJ, respectively. The HRSG heat exchangers share the same fuel cost (7.49 $/GJ), and their product costs range from 10.81 $/GJ (superheater 2) to 13.81 $/GJ (screen).

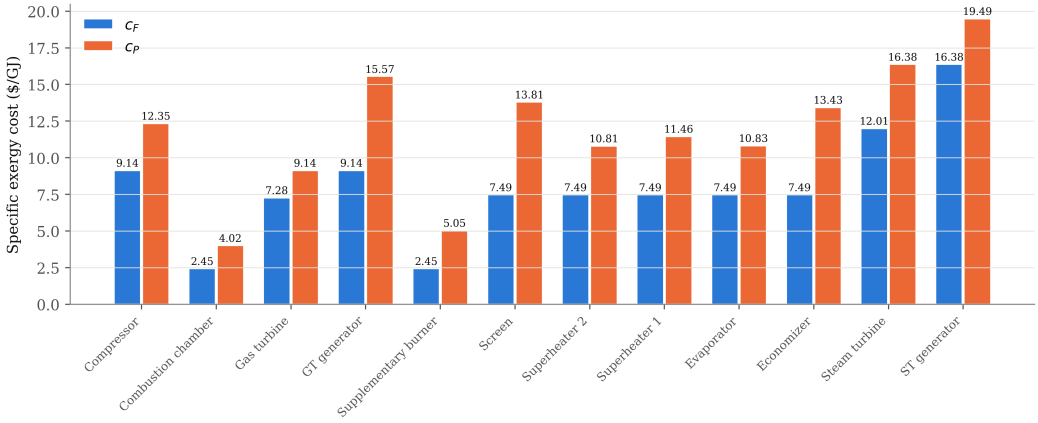


Figure 8. Median specific fuel and product costs of the modeled components (analyzed period).

The specific product costs increase across all components, indicating that each process contributes to the cumulative cost of the final electricity. The generators of the gas and steam cycles yield the highest product costs, with medians of 15.57 and 19.49 $/GJ, respectively. The median specific exergy cost of the electricity delivered by the plant in the analyzed period was 16.47 $/GJ.

The specific exergy cost of electricity decreases as the gross electrical power output, $\dot{W}_{\mathrm{gross}}$, increases, as shown in Figure 9, where each marker represents one operating point and the black line is a quadratic trend curve ($R^2 = 0.995$). The cost decreases from about 21.0 $/GJ at 11.3 MW to about 14.2 $/GJ at 20.9 MW, the highest power observed in the period, and no minimum was found within the observed operating range. This behavior results mainly from the investment cost rate, which is constant in time and is distributed over a larger product as the load increases. The trend curve was not extrapolated beyond the observed range, and it does not result from a formal optimization procedure.

The operating points with the supplementary burner on are concentrated at the highest power outputs and present a lower median electricity cost (15.01 $/GJ at a median power of 18.07 MW) than those with the burner off (17.50 $/GJ at 14.33 MW). This comparison does not isolate the effect of supplementary firing, since the gas turbine also operated at higher loads when the burner was on. To isolate it, the operating points with the gas turbine between 11.5 and 12.5 MW were compared (100 points with the burner off and 315 with the burner on, with median gas turbine power of 11.83 and 12.17 MW and median ambient temperatures of 31.0 and 30.3 °C, respectively).

In this range, supplementary firing increased the median electrical output from 15.98 to 18.10 MW with an additional heat input of 4.58 MW, i.e., an incremental efficiency of about 46%, practically equal to the plant efficiency (46.9% in both groups). As a result, the median cost of electricity decreased from 16.19 to 14.99 $/GJ (−7.4%), because the investment cost rate of the plant, which does not depend on supplementary firing, is distributed over a larger product, whereas the additional fuel is converted at an efficiency similar to that of the plant. Therefore, under the analyzed conditions, supplementary firing reduced the cost of electricity despite its exergy destruction. This conclusion depends on the incremental efficiency of supplementary firing remaining close to the plant efficiency, and it should be reassessed for other gas turbine loads and economic parameters.

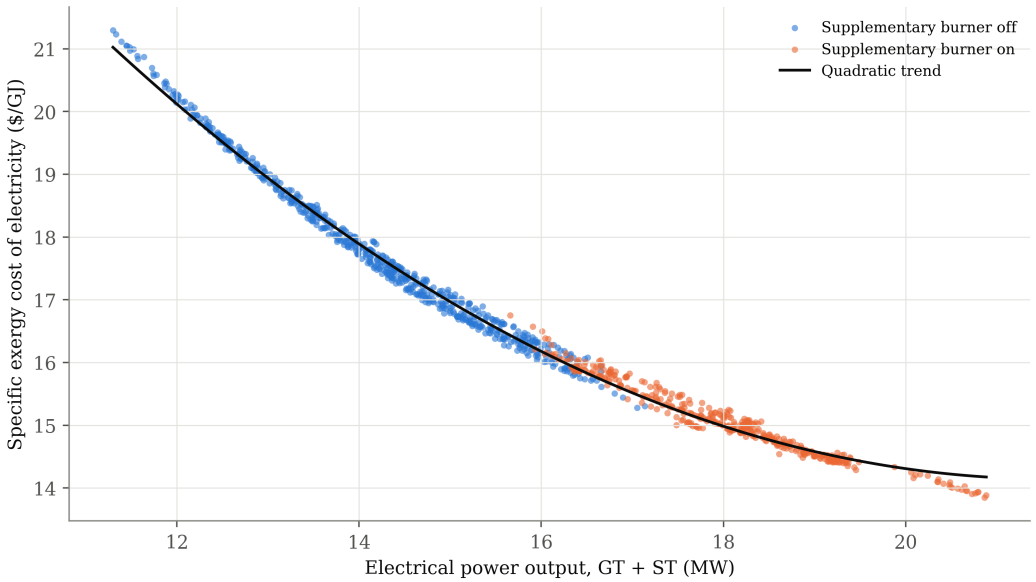


Figure 9. Specific exergy cost of electricity as a function of the gross electrical power output (analyzed period).

The exergoeconomic performance indicators of the period are summarized in Table 11, where the components are arranged in ascending order of the median relative cost difference, r_k. This parameter quantifies the extent to which the specific product cost exceeds the specific fuel cost. For example, in the ST generator, the product cost is 19% higher than the fuel cost, the lowest relative increase among the components.

Table 11. Median relative cost difference and exergoeconomic factor of the modeled components in the analyzed period (interquartile range in parentheses). For the supplementary burner, only the 407 operating points with the burner on are considered.

Component	r_k	f_k
ST generator	0.19 (0.18–0.19)	0.41 (0.39–0.42)
Gas turbine	0.26 (0.24–0.28)	0.75 (0.73–0.76)
Steam turbine	0.33 (0.26–0.35)	0.35 (0.34–0.39)
Compressor	0.35 (0.33–0.36)	0.81 (0.79–0.86)
Superheater 2	0.41 (0.35–0.44)	0.82 (0.75–0.83)
Evaporator	0.46 (0.45–0.47)	0.59 (0.55–0.61)
Superheater 1	0.52 (0.50–0.53)	0.61 (0.55–0.63)
Combustion chamber	0.64 (0.63–0.65)	0.21 (0.21–0.23)
GT generator	0.70 (0.68–0.75)	0.96 (0.95–0.96)
Economizer	0.79 (0.78–0.82)	0.60 (0.58–0.61)
Screen	0.84 (0.74–0.96)	0.22 (0.20–0.25)
Supplementary burner	1.06 (0.90–1.45)	0.39 (0.30–0.54)

The largest values of r_k are associated with the supplementary burner ($r_k = 1.06$), the screen (0.84), and the economizer (0.79), followed by the GT generator (0.70) and the combustion chamber (0.64). In the supplementary burner and in the screen, the relative cost increase is due mainly to exergy destruction, whereas in the GT generator it is due to the investment cost. The supplementary burner also presents the widest interquartile range (0.90–1.45), because its exergy efficiency and product depend on its heat input, which varied widely in the period.

The exergoeconomic factor, f_k, also presented in Table 11, represents the ratio between the component cost rate and the sum of the component cost rate and the cost rate associated

with exergy destruction. Low values of f_k indicate that the total cost of the component is dominated by thermodynamic irreversibilities rather than by capital investment.

The combustion chamber ($f_k = 0.21$) and the screen (0.22) present the lowest values, followed by the steam turbine (0.35), the supplementary burner (0.39), and the ST generator (0.41), indicating that efforts to reduce irreversibilities in these components are likely to provide greater economic benefits than increases in equipment investment. In contrast, the GT generator (0.96), superheater 2 (0.82), the compressor (0.81), and the gas turbine (0.75) are dominated by investment costs.

4. Conclusions

This study presented a comprehensive analysis of the combined-cycle power plant through energy, exergy, and exergoeconomic modeling, with the objective of evaluating its performance, identifying the main sources of irreversibility, and determining the cost of electricity generation within the context of energy and exergy conversion processes.

The model was applied to 1027 steady-state operating points recorded over one month of operation. The comparison with operational data showed that the steam production calculated from the energy balances of the gas turbine and HRSG agrees with the measured steam flow rate, with a mean absolute percentage error of 2.8%, and that the exhaust gas temperatures between the HRSG sections are reproduced with root mean square errors between 4 and 13 °C.

The exergy analysis revealed that exergy destruction occurs predominantly in the combustion chamber, which accounted for 63.5% and 57% of the total exergy destruction without and with supplementary firing, respectively. The mean exergy destruction rate was 17.10 MW without supplementary firing and 21.16 MW with it.

In the operating condition without supplementary firing, the gas cycle accounted for 81% of the total exergy destruction, while the steam cycle contributed 19%. When the supplementary burner was activated, the contribution of the steam cycle increased to 28%, mainly because of the irreversibilities of the supplementary combustion (7.5% of the total).

The combined cycle achieved median gross first- and second-law efficiencies of 46.6% and 44.6%, respectively, and 45.1% and 43.2% when the auxiliary consumption of the plant (median of 3.2% of the gross power) is discounted. These values are similar to those reported for large natural gas combined-cycle plants in operation [28,29]. Among the main turbomachinery components, the gas turbine exhibited a median exergy efficiency of 94%, whereas the steam turbine reached 83%.

The specific exergy cost of electricity decreased with the plant load, from about 21.0 $/GJ at 11.3 MW to about 14.2 $/GJ at 20.9 MW, the highest load observed, with a median of 16.47 $/GJ in the period. This behavior results mainly from the distribution of the investment cost rate, which accounts for about 62% of the total cost rate, over a larger product. At the representative operating point, the cost of electricity was 13.98 $/GJ, and it varied by ±18.9% for a ±50% change in the natural gas price.

The exergoeconomic indicators showed that the highest median relative cost differences were associated with the supplementary burner ($r_k = 1.06$), the screen (0.84), and the economizer (0.79), whereas the combustion chamber, with $r_k = 0.64$, presented the highest cost rate associated with exergy destruction. At the same gas turbine load, supplementary firing increased the electrical output by about 2.1 MW with an incremental efficiency of about 46%, similar to that of the plant, and reduced the median cost of electricity by 7.4%. The low exergoeconomic factors of the combustion chamber (0.21), screen (0.22), and supplementary burner (0.39) indicate that reducing their irreversibilities is the most effective way to reduce the cost of electricity, whereas the turbomachinery and generators are dominated by investment costs.

Since all the investment costs are academic estimates based on literature correlations, the absolute values of the exergoeconomic indicators should be interpreted as estimates. The sensitivity analysis showed that the electricity cost is strongly influenced by economic assumptions, increasing by 18.9% for a 50% increase in natural gas price, by 18.7% for a 30% increase in equipment costs, and by 26.7% when annual operating hours decrease to 70% of the reference value. Alternative HRSG cost allocation methods had a negligible impact on the overall electricity cost but affected component-level indicators. Although the distinction between investment-dominated and exergy-destruction-dominated components remained consistent, the component with the highest relative cost difference varied across scenarios. Further analyses at different operating conditions are needed to assess the robustness of these findings.

The results correspond to the operating conditions of the analyzed period and may vary with changes in demand, maintenance interventions, and the replacement of equipment; the model, however, can be applied to other periods with the corresponding operational data.

The developed model provides detailed information regarding the thermodynamic and economic performance of the plant and can be used to evaluate operational strategies and identify opportunities for performance improvement. In particular, the substantial exergy destruction observed in the initial components of the gas cycle highlights the importance of reducing irreversibilities in these units.

Overall, the integrated energy, exergy, and exergoeconomic modeling approach proved to be an effective tool for evaluating both the efficiency and the economic viability of combined-cycle power plants. The results contribute to a better understanding of the relationship between thermodynamic performance and cost formation, providing useful support for operational assessment, decision-making, and strategic planning in thermoelectric power generation systems.

Author Contributions: Methodology, (G.B.L., J.A.S., L.H., J.J.V.F., J.V.S.d.A., T.G.S.d.L., J.A.d.L. and G.A.A.M.); software, (G.B.L., J.A.S., L.H., J.J.V.F. and J.V.S.d.A.); validation, (G.B.L., J.A.S., L.H., J.J.V.F., J.V.S.d.A., J.A.d.L., G.A.A.M., A.V.d.S.N., J.M.M.V., E.C.T.d.M. and T.G.S.d.L.); formal analysis (G.B.L., J.A.S., L.H., J.J.V.F., J.V.S.d.A., J.A.d.L., G.A.A.M., A.V.d.S.N., S.L.C., J.M.M.V., E.C.T.d.M. and T.G.S.d.L.). All authors have read and agreed to the published version of the manuscript.

Funding: The authors would like to thank the R&D&I program of the Brazilian Electricity Regulatory Agency (ANEEL) for the financial support (R&D&I project PD-00498-2301/2023). They also thank EMBRAPII CEAR/UFPB for the technical and financial support necessary for the completion of this work.

Data Availability Statement: Restrictions apply to the availability of these data. The data were obtained from a third-party company and are available from the authors with the permission of the data provider.

Conflicts of Interest: The authors declare no conflicts of interest.

Nomenclature

Symbols

a_{st}	stoichiometric oxygen requirement (kmol O_2/kmol fuel)
AFR	air–fuel ratio (kg/kg)
b, c	moles of N_2 and H_2O per mole of O_2 in the humid air
c	specific exergy cost ($/GJ)
$\dot{C}$	cost rate ($/h)
$\dot{E}_F$, $\dot{E}_P$, $\dot{E}_D$	fuel, product, and destruction exergy rates of a component (MW)
f_k	exergoeconomic factor (–)

h	specific enthalpy (kJ/kg)
i	annual interest rate (–)
M	molar mass (kg/kmol)
$\dot{m}$	mass flow rate (kg/s)
n_{h}	annual operating time (h)
n_{years}	plant lifetime (years)
p	pressure (kPa)
q	steam quality (–)
$\dot{Q}$	heat transfer rate (MW)
r_k	relative cost difference (–)
s	specific entropy (kJ/(kg·K))
S	component capacity used in the cost scaling
T	temperature (°C or K)
w	specific work (kJ/kg)
$\dot{W}$	power (MW)
x	specific exergy (kJ/kg)
$\dot{X}$	exergy rate of a stream (MW)
$\dot{Z}$	component cost rate ($/h)
Greek symbols	
α	cost scaling exponent (–)
γ	maintenance factor (–)
η_{I}, η_{II}	first- and second-law efficiencies (–)
η_{ex}	exergy efficiency of a component (–)
η_{gen}	generator efficiency (–)
λ	excess air ratio (–)
ϕ	ratio of the chemical exergy to the LHV of the fuel (–)
Subscripts	
0	dead state
1–49, bd	states of Figure 1 (bd: drum blowdown)
aux	auxiliary consumption
CC, *SB*	combustion chamber, supplementary burner
Comp, *GT*, *ST*	compressor, gas turbine, steam turbine
D	exergy destruction
e, *w*	electrical power, shaft work (states 3w, 7w, 7e, 42w, 42e)
EG, *NG*	exhaust gas, natural gas
F, P	fuel, product
GC	gas cycle
gross, *net*	gross and net electrical power
HX	heat exchanger
in, *out*	inlet, outlet
k	component
s	isentropic state
sat	saturation
st	stoichiometric
Abbreviations	
CCGT	combined-cycle gas turbine
CEPCI	Chemical Engineering Plant Cost Index
CRF	capital recovery factor
DSH	desuperheater
HRSG	heat recovery steam generator

LHV	lower heating value
MAPE	mean absolute percentage error
PEC	purchase equipment cost
RMSE	root mean square error
SPECO	specific exergy costing

References

1. Wang, L.; Jiang, B.; Shi, Y.; Chen, Z. Adaptive robust unit commitment of combined-cycle gas-turbine considering mode-based modeling of carbon capture plant. *IEEE Access* **2023**, *11*, 34510–34528. https://doi.org/10.1109/ACCESS.2023.3264833.
2. Rao, A. Natural gas-fired combined cycle (ngcc) systems. In *Combined Cycle Systems for Near-Zero Emission Power Generation*; Elsevier: Amsterdam, The Netherlands, 2012; pp. 103–128.
3. Çengel, Y.; Boles, M. *Termodinâmica*, 7th ed.; Bookman Editora: Porto Alegre, RS, Brazil, 2013.
4. Liu, Z.; Karimi, I. Simulation and optimization of a combined cycle gas turbine power plant for part-load operation. *Chem. Eng. Res. Des.* **2018**, *131*, 29–40.
5. Yu, J.; Petersen, N.; Liu, P.; Li, Z.; Wirsum, M. Hybrid modelling and simulation of thermal systems of in-service power plants for digital twin development. *Energy* **2022**, *260*, 125088. https://doi.org/10.1016/j.energy.2022.125088.
6. Bishal, S.S.; Faysal, D.F.; Ehsan, M.M.; Salehin, S. Performance evaluation of an integrated cooling and power system combining supercritical CO_2, gas turbine, absorption refrigeration, and organic rankine cycles for waste energy recuperating system. *Results Eng.* **2023**, *17*, 100943. https://doi.org/10.1016/j.rineng.2023.100943.
7. Lugo-Leyte, R.; Salazar-Pereyra, M.; Bonilla-Blancas, A.E.; Lugo-Mendez, H.D.; Ruíz-Ramírez, O.A.; Toledo-Velázquez, M. Exergetic Analysis of Triple-Level Pressure Combined Power Plant with Supplementary Firing. *J. Energy Eng.* **2016**, *142*, 05016001. https://doi.org/10.1061/(ASCE)EY.1943-7897.0000348.
8. Ahmadi, P.; Dincer, I.; Rosen, M.A. Exergy, exergoeconomic and environmental analyses and evolutionary algorithm based multi-objective optimization of combined cycle power plants. *Energy* **2011**, *36*, 5886–5898. https://doi.org/10.1016/j.energy.2011.08.034.
9. Lazzaretto, A.; Tsatsaronis, G. SPECO: A systematic and general methodology for calculating efficiencies and costs in thermal systems. *Energy* **2006**, *31*, 1257–1289. https://doi.org/10.1016/j.energy.2005.03.011.
10. Moran, M.J.; Shapiro, H.N.; Boettner, D.D.; Bailey, M.B. *Fundamentals of Engineeringthermodynamics*; John Wiley & Sons: Hoboken, NJ, USA, 2018.
11. Wagner, W.; Pruß, A. The iapws formulation 1995 for the thermodynamic properties of ordinary water substance for general and scientific use. *J. Phys. Chem. Ref. Data* **2002**, *31*, 387–535. https://doi.org/10.1063/1.1461829.
12. Arpit, S.; Das, P. A state-of-the-art review of heat recovery steam generators and waste heat boilers. *Energy Effic.* **2023**, *16*, 99. https://doi.org/10.1007/s12053-023-10179-5.
13. Bejan, A.; Tsatsaronis, G.; Moran, M. *Thermal Design and Optimization*; Wiley-Interscience: New York, NY, USA, 1996.
14. Altarawneh, O.R.; Alsarayreh, A.A.; Al-Falahat, A.M.; Al-Kheetan, M.J.; Alrwashdeh, S.S. Energy and exergy analyses for a combined cycle power plant in jordan. *Case Stud. Therm. Eng.* **2022**, *31*, 101852. https://doi.org/10.1016/j.csite.2022.101852.
15. Chang, R.; Goldsby, K.A. *Química*; AMGH Editora: Porto Alegre, RS, Brazil, 2013
16. Pinto, G.M. Análise Termoeconômica de uma Central de Ciclo Combinado de 826 MW—Estudo de Caso Utilizando um Simulador Full-Scope. Master's Thesis, Universidade Federal de Itajubá, Itajubá, MG, Brazil, 2020. Available online: https://repositorio.unifei.edu.br/jspui/bitstream/123456789/2340/3/Disserta%C3%A7%C3%A3o_2021062.pdf (accessed on 17 September 2026).
17. *ISO 6976:2016*; Natural Gas—Calculation of Calorific Values, Density, Relative Density and Wobbe Indices from Composition. International Organization for Standardization: Geneva, Switzerland, 2016.
18. Branco, F.P. Análise termoeconômica de uma usina termelétrica a gás natural operando em ciclo aberto e em ciclo combinado. Master's Thesis, Universidade Estadual Paulista (UNESP), Faculdade de Engenharia de Ilha Solteira, Ilha Solteira, SP, Brazil, 2005. Available online: https://hdl.handle.net/11449/321200 (accessed on 17 September 2026).
19. Gogoi, T.; Lahon, D.; Nondy, J. Energy, exergy and exergoeconomic (3E) analyses of an organic Rankine cycle integrated combined cycle power plant. *Therm. Sci. Eng. Prog.* **2023**, *41*, 101849. https://doi.org/10.1016/j.tsep.2023.101849.
20. Brodrick, P.G.; Kang, C.A.; Brandt, A.R.; Durlofsky, L.J. Optimization of carbon-capture-enabled coal-gas-solar power generation. *Energy* **2015**, *79*, 149–162. https://doi.org/10.1016/j.energy.2014.11.003.
21. Kang, C.A.; Brandt, A.R.; Durlofsky, L.J. Optimizing heat integration in a flexible coal–natural gas power station with CO_2 capture. *Int. J. Greenh. Gas Control* **2014**, *31*, 138–152. https://doi.org/10.1016/j.ijggc.2014.09.019.
22. Silva, M.M. Repotenciamento em sistemas de geração de potência na indústria siderúrgica utilizando análise termoeconômica. Ph.D. Thesis, Universidade Federal de Itajubá, Itajubá, MG, Brazil, 2004.
23. Garrett, D.E. *Chemical Engineering Economics*; Springer Science & Business Media: Berlin/Heidelberg, Germany, 2012.

24. Petrakopoulou, F.; Boyano, A.; Cabrera, M.; Tsatsaronis, G. Exergoeconomic and exergoenvironmental analyses of a combined cycle power plant with chemical looping technology. *Int. J. Greenh. Gas Control* **2011**, *5*, 475–482. Available online: https://www.sciencedirect.com/science/article/pii/S1750583610001064 (accessed on 17 September 2026).
25. Shirmohammadi, R.; Aslani, A.; Ghasempour, R.; Romeo, L.M.; Petrakopoulou, F. Exergoenvironmental analysis and thermoeconomic optimization of an industrial post-combustion CO_2 capture and utilization installation. *J. CO_2 Util.* **2022**, *59*, 101927.
26. Ulrich, G.D. *A Guide to Chemical Engineering Process Design and Economics*; Wiley: New York, NY, USA, 1984.
27. Gomes, C.M. Análise termodinâmica, exergética e termoeconômica de uma instalação termelétrica em ciclo combinado, com cogeração de vapor. Ph.D. Thesis, Universidade Federal de Itajubá, Itajubá, MG, Brazil, 2001.
28. Elwardany, M.; Nassib, A.M.; Mohamed, H.A.; Abdelaal, M.R. Energy and exergy assessment of 750 MW combined cycle power plant: A case study. *Energy Nexus* **2023**, *12*, 100251. https://doi.org/10.1016/j.nexus.2023.100251.
29. Bataineh, K.; Khaleel, B.A. Thermodynamic analysis of a combined cycle power plant located in Jordan: A case study. *Arch. Thermodyn.* **2020**, *41*, 95–123. https://doi.org/10.24425/ather.2020.132951.
30. Ersayin, E.; Ozgener, L. Performance analysis of combined cycle power plants: A case study. *Renew. Sustain. Energy Rev.* **2015**, *43*, 832–842. https://doi.org/10.1016/j.rser.2014.11.082.

Disclaimer/Publisher's Note: The statements, opinions and data contained in all publications are solely those of the individual author(s) and contributor(s) and not of MDPI and/or the editor(s). MDPI and/or the editor(s) disclaim responsibility for any injury to people or property resulting from any ideas, methods, instructions or products referred to in the content.